Article

Cell Reports

Structural Dynamics of the YidC:Ribosome Complex during Membrane Protein Biogenesis

Graphical Abstract

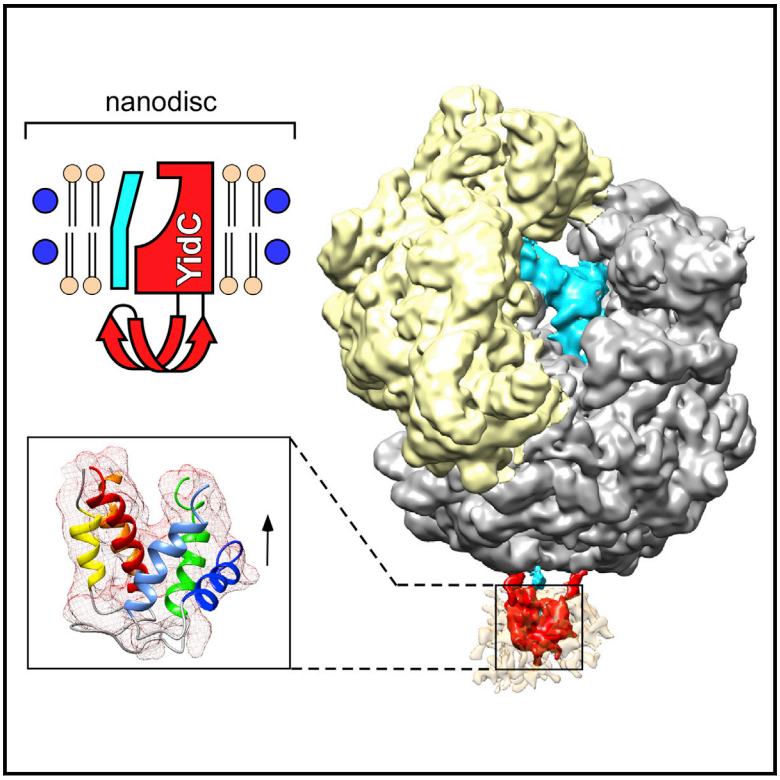

Authors

Alexej Kedrov, Stephan Wickles, Alvaro H. Crevenna, ..., Otto Berninghausen, Don C. Lamb, Roland Beckmann

Correspondence

kedrov@genzentrum.lmu.de (A.K.), beckmann@genzentrum.lmu.de (R.B.)

In Brief

Kedrov et al. use a combination of biochemical, biophysical, and structural approaches to study the insertase YidC in its native lipid environment upon interaction with ribosomes. The results describe how YidC recognizes translating ribosomes and changes its conformation upon nascent chain insertion.

Highlights

- YidC:ribosome assembly strongly depends on the nascent chain length
- Gel phase membranes allow the transient YidC:nascent chain complex to be stabilized
- Single-particle cryo-EM reveals the structure of ribosome-bound YidC in nanodiscs
- YidC undergoes a conformational change upon co-translational substrate insertion

Accession Numbers

5M5H

Kedrov et al., 2016, Cell Reports *17*, 2943–2954
December 13, 2016
http://dx.doi.org/10.1016/j.celrep.2016.11.059

CellPress

Cell Reports
Article

Structural Dynamics of the YidC:Ribosome Complex during Membrane Protein Biogenesis

Alexej Kedrov,[1,*] Stephan Wickles,[1] Alvaro H. Crevenna,[2] Eli O. van der Sluis,[1] Robert Buschauer,[1] Otto Berninghausen,[1] Don C. Lamb,[2,3] and Roland Beckmann[1,3,4,*]

[1]Gene Center Munich, Department of Biochemistry, Ludwig-Maximilians-University Munich, Feodor-Lynen-Strasse 25, Munich 81377, Germany

[2]Physical Chemistry, Department of Chemistry, Center for Nanoscience (CeNS), the NanoSystems Initiative Munich (NIM), Ludwig-Maximilians-University Munich, Butenandtstrasse 11, Munich 81377, Germany

[3]Center for Integrated Protein Science Munich (CiPSM), Ludwig-Maximilians-University, Butenandtstrasse 5-13, Munich 81377, Germany

[4]Lead Contact

*Correspondence: kedrov@genzentrum.lmu.de (A.K.), beckmann@genzentrum.lmu.de (R.B.)

http://dx.doi.org/10.1016/j.celrep.2016.11.059

SUMMARY

Members of the YidC/Oxa1/Alb3 family universally facilitate membrane protein biogenesis, via mechanisms that have thus far remained unclear. Here, we investigated two crucial functional aspects: the interaction of YidC with ribosome:nascent chain complexes (RNCs) and the structural dynamics of RNC-bound YidC in nanodiscs. We observed that a fully exposed nascent transmembrane domain (TMD) is required for high-affinity YidC:RNC interactions, while weaker binding may already occur at earlier stages of translation. YidC efficiently catalyzed the membrane insertion of nascent TMDs in both fluid and gel phase membranes. Cryo-electron microscopy and fluorescence analysis revealed a conformational change in YidC upon nascent chain insertion: the essential TMDs 2 and 3 of YidC were tilted, while the amphipathic helix EH1 relocated into the hydrophobic core of the membrane. We suggest that EH1 serves as a mechanical lever, facilitating a coordinated movement of YidC TMDs to trigger the release of nascent chains into the membrane.

INTRODUCTION

Membrane protein biogenesis is a vital and fundamental cellular process that includes membrane targeting, insertion, and assembly of 25%–30% of all proteins found in living organisms. While universal principles of the membrane protein biogenesis have been extensively investigated over the last decade and comprehensive studies have addressed molecular mechanisms of the Sec translocon in great detail (du Plessis et al., 2011; Park and Rapoport, 2012), relatively little is known about the functional mechanisms of the essential YidC/Oxa1/Alb3 membrane insertase family (Saller et al., 2012). Either alone or in association with the Sec translocon, these conserved insertases are involved in the biogenesis of essential membrane proteins (Samuelson et al., 2000; Scotti et al., 2000; van der Laan et al., 2004). An important milestone has been recently reached, as crystal structures of YidC proteins from *Bacillus halodurans* and *Escherichia coli* have been solved (Kumazaki et al., 2014a, 2014b). These structures describe the organization of the membrane-embedded insertase as a conserved bundle of five transmembrane (TM) helices forming a hydrophilic groove at the cytoplasmic side (Figure 1). The groove reaches halfway to the periplasmic side and provides the path for the substrate; i.e., nascent membrane protein upon its insertion. Initial substrate recognition is believed to occur at the cytoplasmic helical hairpin CH1-CH2 that connects TM2 and TM3 in *E. coli* YidC and caps the hydrophilic groove of the idle insertase (Kumazaki et al., 2014a, 2014b). Deletions or mutations within CH1-CH2 lead to the loss of cellular viability (Chen et al., 2014; Wickles et al., 2014; Geng et al., 2015). Similarly, deletions within TM2 and TM3 of YidC have lethal effects on cells (Jiang et al., 2003), and these TMs have been described as the functional core of the insertase that interacts with the substrate upon its insertion (Kumazaki et al., 2014a). The non-conserved periplasmic P1 domain found in YidC homologs in many bacteria appears to be non-essential (Jiang et al., 2003), with a remarkable exception for a conserved amphipathic helix EH1 between P1 and TM2, as deletions within EH1 render YidC non-functional both in vivo and in vitro (Jiang et al., 2003; Kumazaki et al., 2014a).

The interaction of YidC with translating ribosomes is likely to constitute an essential stage in co-translational membrane protein insertion that allows partitioning of the hydrophobic nascent chain into the membrane in a direct way. A monomer of YidC interacts with translating ribosomes both in the detergent environment and in the lipid bilayer (Kedrov et al., 2013; Wickles et al., 2014), thus representing the functional insertase unit. Similar to the SecYEG system, YidC specifically interacts with ribosomes that expose hydrophobic nascent chains (Kedrov et al., 2013; Wu et al., 2013). The positively charged C terminus and a short cytoplasmic loop connecting TM4 and TM5 facilitate this interaction (Geng et al., 2015), while the YidC variant lacking the C terminus (YidCΔC) is impaired in ribosome binding (Kedrov et al., 2013).

Recent studies employing single-particle cryo-electron microscopy (cryo-EM) have described the architecture of the detergent-solubilized YidC in complex with translationally stalled ribosomes (Seitl et al., 2014; Wickles et al., 2014). However,

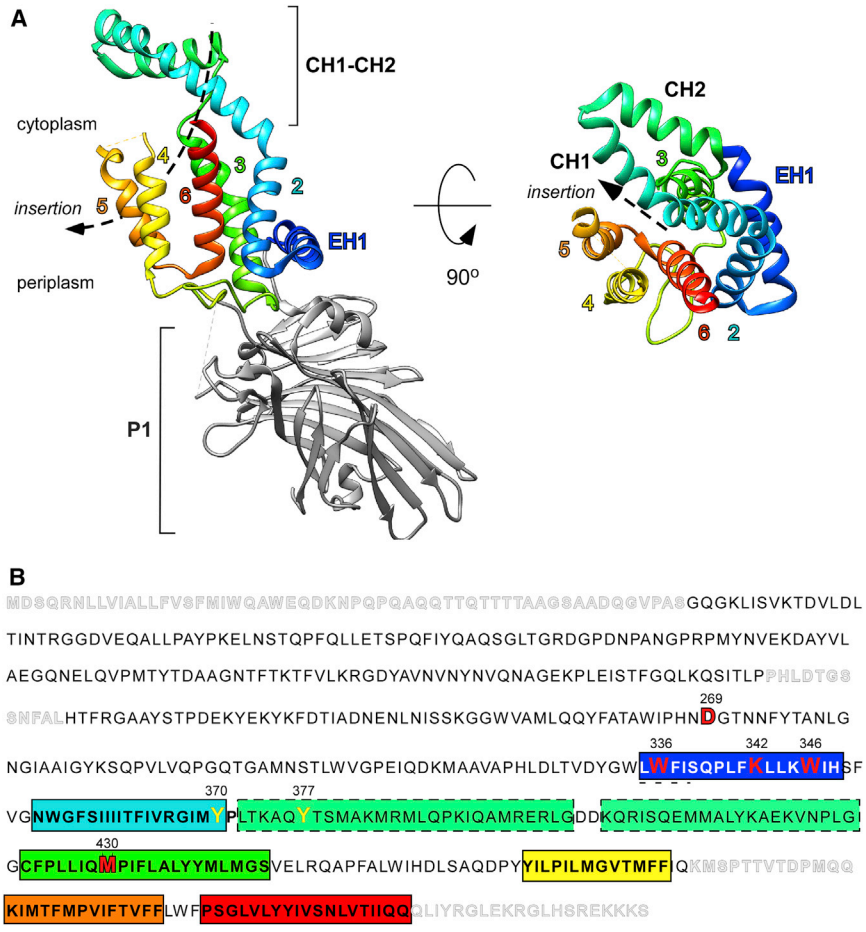

Figure 1. Structure of *E. coli* YidC Membrane Insertase

(A) Structure of YidC in its idle state (PDB ID: 3WVF; Kumazaki et al., 2014b). The essential core of the protein is rainbow colored with domains indicated. The periplasmic domain P1 is shown in gray in the side view and removed in the top view for clarity. A putative insertion path of the nascent chain via the central groove is indicated with a dashed line.

(B) Primary structure of *E. coli* YidC with positions of structural domains indicated. The color coding for domains is the same as in (A). The regions absent in the crystal structure are highlighted in gray. The cytoplasmic CH1-CH2 hairpin is shown with dashed bars. The positions of alanine residues introduced within TM2-CH1 helices are indicated and highlighted in yellow. The positions of cysteine residues introduced for fluorescence and cross-linking analysis are indicated and highlighted in red. The deletion EH1-Δ within the EH1 helix is underlined with a dashed line.

a structural description of the YidC-driven insertion process in the membrane has been lacking. Although several membrane proteins have been meanwhile visualized by cryo-EM in a near physiological lipid environment (Frauenfeld et al., 2011; Efremov et al., 2015; Gao et al., 2016), better structural analysis of YidC:ribosome complex has been hindered by the small size of the insertase (functional core ~30 kDa), by the lack of structural symmetry, its high internal flexibility, and its dynamic mode of ribosome binding. Here, we set out to investigate previously unaccounted determinants of the YidC:ribosome interaction and to build the molecular model of the membrane-embedded YidC:ribosome complex based on cryo-EM and biophysical analysis. Our results demonstrate how the nascent chain and lipid properties influence the YidC:ribosome assembly and document an unexpected conformational change within YidC upon the co-translational substrate insertion.

RESULTS

YidC:Ribosome Interactions Are Dependent on Nascent Chain Length

For investigating YidC:ribosome interactions at the membrane interface, the recombinant YidC was purified, fluorescently labeled, and reconstituted into lipid-based nanodiscs (Denisov et al., 2004; Kedrov et al., 2013) (Figure 2A). For mimicking translating ribosomes, we used stable TnaC-stalled ribosome:nascent chain complexes (RNCs) (Bischoff et al., 2014a) that expose the subunit c of the F_1F_o ATP synthase (F_oc), a model substrate for YidC-mediated insertion (van der Laan et al., 2004). The full-length RNC F_oc-FL contained fully exposed TM1 and the following loop region (Wickles et al., 2014). Binding of the nanodisc-embedded YidC (YidC-ND) to ribosomes was assayed using fluorescence correlation spectroscopy (FCS) by measuring changes in the translational diffusion of the fluorescently labeled YidC-ND (Figure 2B) (Krichevsky and Bonnet, 2002; Wu et al., 2012). Measuring the diffusion time of YidC-ND upon titrating RNC F_oc-FL allowed monitoring the formation of YidC-ND:RNC complexes and revealed the dissociation constant (K_D) of 85 ± 10 nM (Figure 2C). YidC-ND:RNC interactions weakly depended on the membrane composition (Figure 2D), and YidC could efficiently bind RNCs when embedded either in fluid phase (DOPG, DOPE, and DOPC) or gel phase (DPPG and DPPC) lipid membranes. However, removing phosphatidylethanolamine (DOPE) lipids reduced the affinity approximately 3-fold, while reducing the content of phosphatidylglycerol (DOPG) to 20 mol % strongly promoted spontaneous YidC-independent insertion of the nascent chain (Figure S1). Thus, for further analysis of YidC-mediated insertion 30 mol % DOPG was taken as a minimal fraction that simultaneously reflected the natural occupancy of anionic lipids in *E. coli* inner membranes (Cronan, 2003).

We further analyzed the efficiency of the YidC interaction with RNCs bearing shorter nascent chains, thus mimicking earlier stages of membrane protein biogenesis. To investigate the effect of nascent chain length on YidC:ribosome assembly, we generated a set of RNC F_oc, which differed by the length of

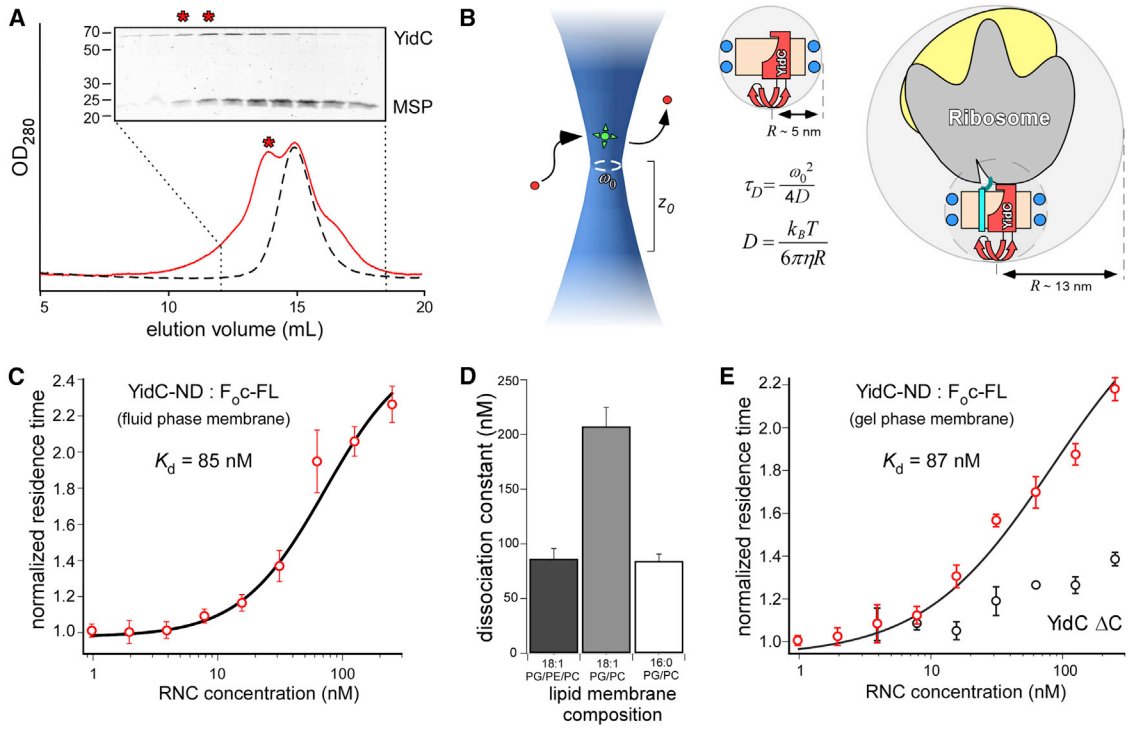

Figure 2. YidC:Ribosome Interactions in Lipid-Based Nanodiscs

(A) Isolation of YidC-ND complexes via size-exclusion chromatography. Due to the size difference, YidC-ND (marked with asterisk; elution volume ~14 mL) elute prior to lipid-loaded, empty nanodiscs (elution volume ~15 mL), so they could be separated from the co-reconstitution reaction (red line). The dashed line shows the elution profile of empty nanodiscs. SDS-PAGE confirms the co-elution of YidC and MSP as constituents of nanodiscs (top).

(B) FCS-based assay of YidC-ND:ribosome interactions. Fluorophore-conjugated YidC molecules diffused through the illuminated confocal volume with the lateral size ω_0 and the vertical size z_0. The average residence time within the focal volume (τ_D) determined from the auto-correlation curve is in inverse proportion to the diffusion coefficient D of YidC that is determined by the hydrodynamic radius of the molecule. The size estimates for free and ribosome-bound YidC-ND are shown.

(C) FCS-based affinity measurement of YidC$^{D269C,\ AF488}$-ND to RNC F_oc-FL in DOPG/DOPE/DOPC-based nanodiscs.

(D) Affinity of the YidC-ND:RNC F_oc-FL complex at different membrane compositions (average + SD).

(E) FCS-based affinity measurements for YidC-ND:RNC F_oc-FL using either full-length YidC or truncated YidCΔC variant reconstituted into nanodiscs with gel phase lipid membranes (35 mol % DPPG and 65 mol % DPPC). Only weak binding was measured for the YidCΔC variant (Kedrov et al., 2013; Geng et al., 2015) that lacks the positively charged C-terminal tail confirming YidC-mediated ribosome binding. See also Figure S1.

solvent-exposed F_oc (Figures 3A and 3B). As the length of the nascent chain decreased, we observed a weaker effect of RNCs on YidC-ND mobility that reflected a decline in binding (Figure 3C). While ~90% of YidC-ND were found in complex with RNC F_oc-FL or F_oc-Δ5, the value dropped to 62% for RNC F_oc-Δ10 and further to 30% for the shortest RNC F_oc-Δ20, which exposed only a fragment of the TM domain (Figure 3D). However, even the weakest YidC:RNC F_oc-Δ20 interactions exceeded binding of YidC-ND to non-translating 70S ribosomes (binding below 10%) or interactions of corresponding RNCs with empty nanodiscs (Figure 3D). We conclude that YidC can recognize and bind ribosome-exposed nascent chains at early stages of translation, while binding efficiency reaches its maximum level once the nascent transmembrane domain is fully exposed outside the ribosomal tunnel.

Nascent Chain Resides at the YidC:Lipid Interface

Upon assembly of the YidC:RNC complex, several scenarios can be envisioned with respect to position of the nascent chain: (1) the nascent chain may reside at the extramembrane interface of YidC, such as the CH1-CH2 hairpin; (2) it can be partially inserted and docked into the central hydrophilic groove of YidC; (3) it could be fully inserted into the bilayer and retain contact with YidC; or (4) it can transiently interact with YidC for insertion and then be released into the lipid bilayer. To probe the position of the nascent chain within the formed YidC-ND:RNC complex, we used the disulphide cross-linking approach that was previously employed to analyze interactions of YidC both with co- and post-translationally inserted substrates (Yu et al., 2008). A single-cysteine F_oc^{G23C}-FL nascent chain has been shown to cross-link with YidC^{M430C} in the detergent-solubilized state resulting in a product of ~100 kDa. Thus, the nascent chain is positioned in proximity to TM3 after the YidC:ribosome complex has assembled (Wickles et al., 2014). The cross-linked product was also observed when YidC^{M430C} was reconstituted into nanodiscs with 30 mol % DOPG, 30 mol % DOPE, and 40 mol % DOPC lipids, and the efficiency of cross-linking depended on the position of the cysteine within the nascent chain (Figure 4A).

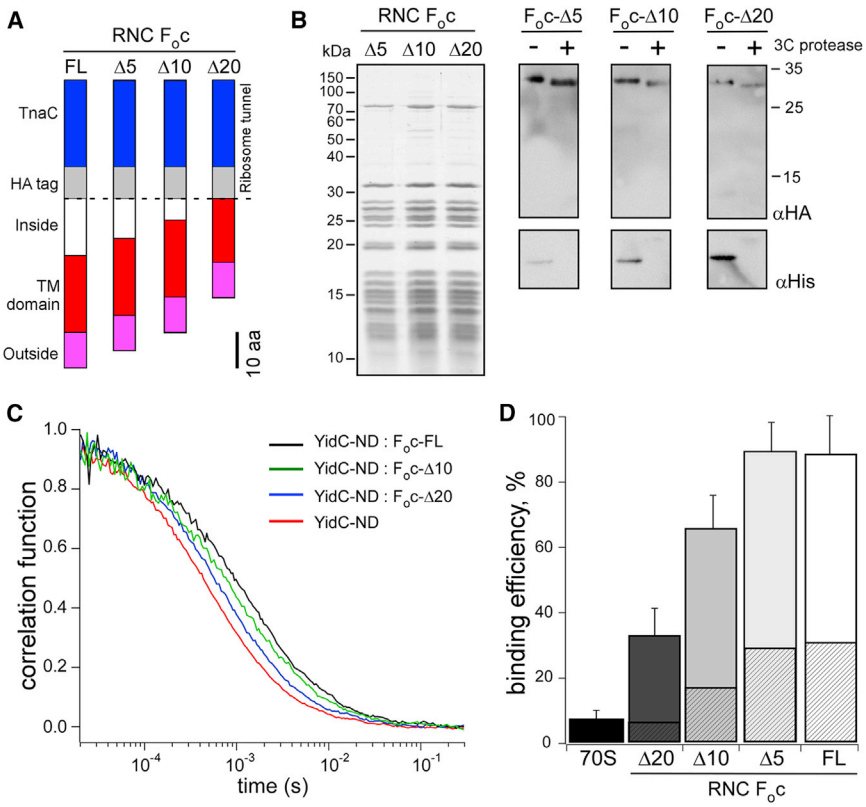

Figure 3. The Nascent Chain Length Determines YidC:Ribosome Interactions

(A) The set of F_oc nascent chains mimicking early stages of the protein synthesis. The reduction in length is achieved by stepwise shortening the cytoplasmic domain of F_oc ("Inside") and for F_oc-Δ20, first transmembrane domain ("TM domain").

(B) SDS-PAGE (left) and western blot (right) of newly designed RNCs. The N-terminal hexahistidine tag at the nascent chains was removed via 3C protease cleavage during the RNC purification.

(C) FCS auto-correlations traces of YidC$^{D269C, AF488}$-ND upon interactions with different RNC F_oc constructs.

(D) Binding efficiency of YidC-ND to 150 nM RNCs and non-programmed ribosomes as determined from FCS (solid bars, average + SD). The binding efficiency of empty ND to RNCs due to the spontaneous membrane insertion of the nascent chain is shown by striped bars.

Cysteines at positions 23 and 24 of F_oc resulted in the cross-linked product, while no product was detected if a cysteine was introduced at a proximate position 22. As placing a cysteine at different positions within F_oc did not influence YidC:ribosome interactions (Figure 4A), the pronounced difference in YidC cross-linking efficiencies observed between F_oc^{I22C} and F_oc^{G23C}/F_oc^{A24C} was likely due to a preferred orientation of the nascent chain relative to the ribosome-bound YidC. Thus, we concluded that the TM domain of the nascent chain was fully inserted into the membrane by YidC and could still be found contacting YidC in a distinct orientation proximate to TM3.

When conducting YidC:nascent chain proximity analysis, we reproducibly observed that, in spite of the high affinity of YidC-ND:ribosome complexes, the cross-linking occurred less efficiently in nanodiscs than in the detergent environment (Figure 4B). That difference could either indicate poor membrane partitioning of the nascent chain or a high degree of freedom and potential lateral diffusion of the inserted nascent chain within the nanodisc, but not within the detergent micelle. In agreement with the latter hypothesis and pointing toward structural heterogeneity, a cryo-EM reconstruction of the YidC-ND:ribosome complex in DOPG/DOPE/DOPC lipids showed no extra density for YidC-ND at the expected position close to the tunnel exit (data not shown). Thus, we set out to form a stable complex by modulating the properties of the membrane. First, we reduced the dimensions of the nanodisc by using a truncated variant of the scaffold protein, MSP1D1-ΔH5 (Hagn et al., 2013; Kucharska et al., 2015) (Figure S2). The inner diameter of these nanodiscs was estimated to be approximately 6 nm (Hagn et al., 2013), and hence a YidC monomer, which has the largest dimensions at the cytoplasmic interface of ~3 nm, would occupy ~25% of the surface area, and thus still allow for putative conformational dynamics and insertion of the substrate nascent chain. Second, we reduced the fluidity of the lipid bilayer by using gel phase lipids (DPPG/DPPC), which supported YidC:ribosome complex assembly (Figure 1D). To that end, cross-linking of the F_oc^{G23C}-FL nascent chain to YidC was substantially enhanced when using the modified system (Figure 4B), and the greater occupancy was likely due to reduced lateral diffusion in the gel phase membrane. Remarkably, efficient YidC:ribosome complex assembly (K_D ~200 nM) and cross-linking to YidC was also observed for the shorter nascent chain F_oc^{G23C}-Δ10 (Figures 4C and 4D), indicating that the hydrophobic TM domain could be inserted into the bilayer at early stages of F_oc biogenesis.

Structure of the YidC-ND:RNC Complex

Current knowledge of the YidC:ribosome complex architecture is largely based on cryo-EM structures observed in the detergent environment (Seitl et al., 2014; Wickles et al., 2014). As detergents are known to greatly affect interactions of ribosomes with YidC (Kedrov et al., 2013), we set out to study the YidC:ribosome structure in near physiological lipid membranes of nanodiscs. To ensure a tight docking of the ribosome on the insertase and to reduce YidC-independent spontaneous partitioning of the nascent chain, a truncated variant of the nascent chain, F_oc-Δ10, was employed, and DPPG/DPPC lipids were used to form YidC-containing nanodiscs. This YidC-ND:RNC was subjected to cryo-EM and single-particle analysis for structure determination. In silico sorting yielded a stable subset of particles (Figure S3), and the reconstruction showed a density both for tRNA in the ribosomal P-site and an additional density

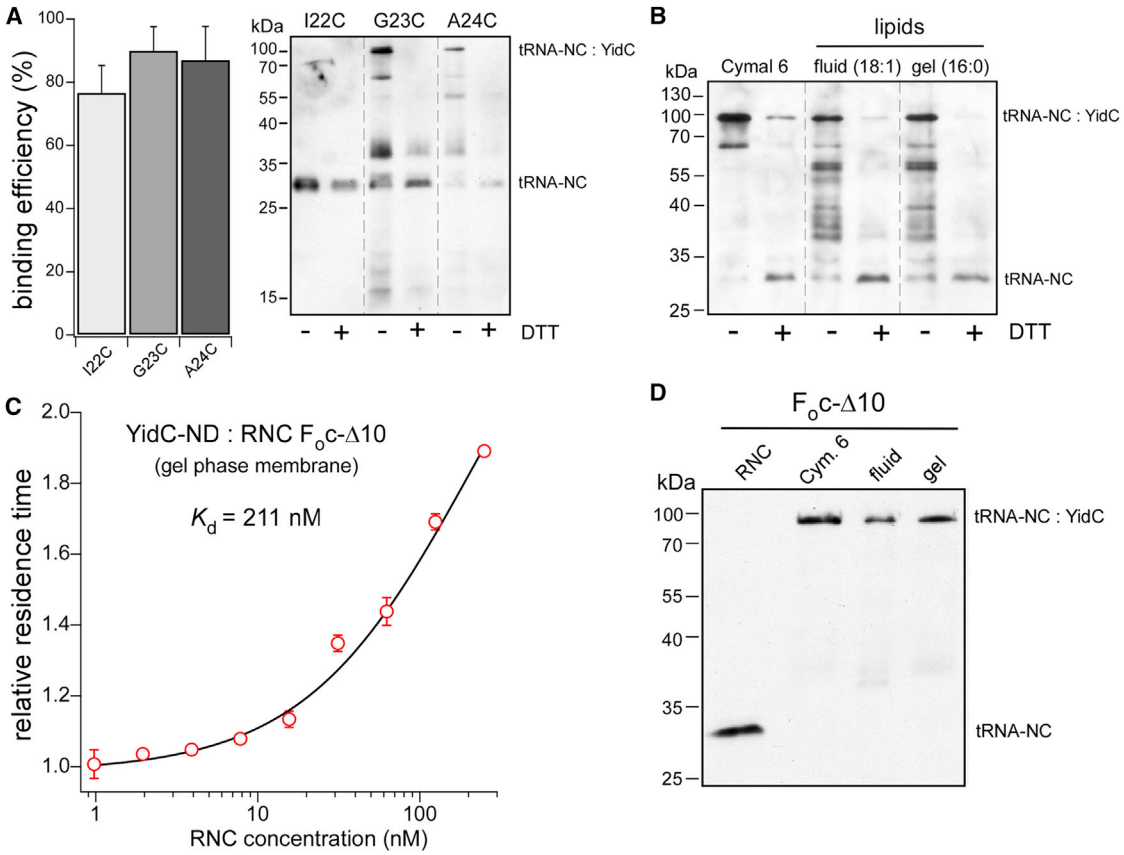

Figure 4. YidC-Mediated Membrane Insertion of the Nascent Chain

(A) Left: binding efficiency of YidC-ND to RNC F_oc-FL measured by FCS is not affected by a single-cysteine mutation within the nascent chain (average + SD). The efficiency of the cross-linking between the F_oc-FL nascent chain (NC) and $YidC^{M430C}$-ND strongly depends on the position of the cysteine in the nascent chain (right). The YidC-ND was formed using 30 mol % DOPG, 30 mol % DOPE, and 40 mol % DOPC.

(B) Gel phase membrane lipids (DPPG/DPPC; "16:0") within nanodiscs enhance $YidC^{M430C}$:F_oc^{G23C}-FL cross-linking compared to fluid phase membrane lipid (DOPG/DOPE/DOPC; "18:1").

(C) FCS-based affinity measurements of $YidC^{AF488}$-ND to RNC F_oc-Δ10 in DPPG/DPPC gel phase membranes.

(D) Efficient cross-linking between $YidC^{M430C}$ and F_oc^{G23C}-Δ10 nascent chain shows that the short nascent chain can be inserted in DPPG/DPPC-based membranes.

at the tunnel exit for YidC-ND (Figure 5A), which was refined to 3.8 Å resolution for the large ribosomal subunit and 4.5 Å, for the complex with YidC-ND (Figure S3). The intrinsic flexibility of ligands at the ribosomal tunnel was reflected by a lower local resolution for parts of the nanodisc (Figure S4A).

The conserved domain of YidC (EH1-TM2…TM6) was fitted in the prominent density in the core of the nanodisc (Figures 5B and S4; Experimental Procedures). In the resulting model, the C-terminal part of YidC; i.e., TM4, TM5, and TM6, is almost identical to that in the crystallized idle form of YidC and also the detergent-solubilized YidC:RNC complex (Figure 5C). In contrast, the functionally important helices EH1, TM2, and TM3 undergo obvious rearrangements upon ribosome binding and the nascent chain insertion compared to the idle state. In our model, transmembrane helices TM2 and TM3 appear tilted by 9° and 20°, respectively, so the central groove widens substantially, while the amphipathic helix EH1 shifts from the membrane interface into the apolar membrane core. The cytoplasmic side of TM3 is the least resolved element of YidC, which agrees with its high B-factor values observed in available crystal structures (Kumazaki et al., 2014a). An additional helical density was observed close to TM3 and TM5 at the interface of the YidC and the lipid environment (Figure 5B). In agreement with the cross-linking analysis (Figure 4) and previous cryo-EM reconstructions (Wickles et al., 2014), this density has been assigned to the membrane-inserted part of F_oc. Differently from the earlier study, which trapped F_oc at the periphery of YidC (Wickles et al., 2014), in our structure, the newly inserted TM domain is located at the exit of the hydrophilic groove of YidC. The F_oc TM is being held by a pincer-like grip of YidC TM3 and TM5, thus representing an earlier insertion state.

The cryo-EM reconstruction shows two contact points between YidC and the ribosome, which could be interpreted on the basis of the insertase model (Figure S4D). YidC TM6 is positioned in close proximity to ribosomal H59, with a strong connecting density in between, that has been assigned to the

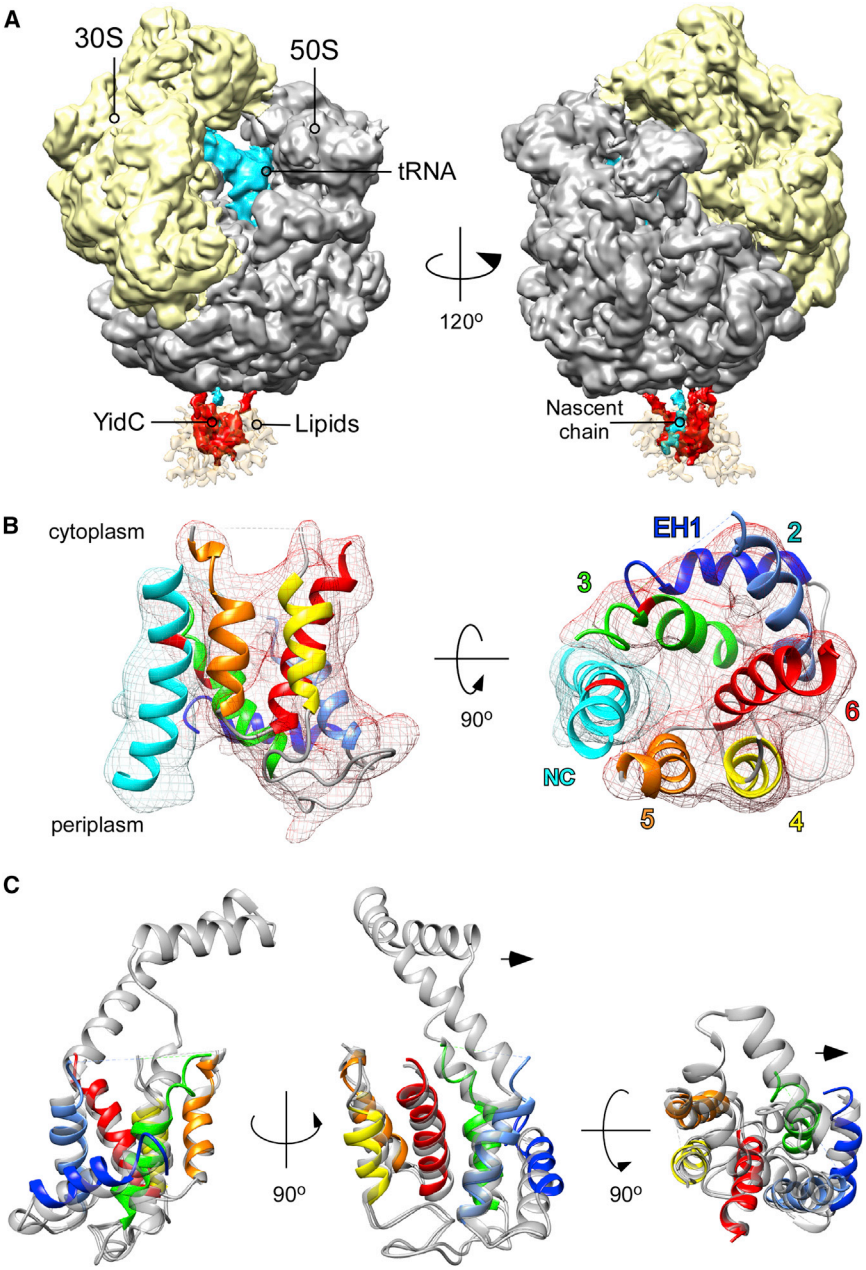

Figure 5. Cryo-EM Reconstruction of the YidC-ND:RNC F_oc Complex

(A) Electron density of the YidC-ND:RNC F_oc-Δ10 complex, with 30S ribosome subunit in yellow, 50S in gray, tRNA and the F_oc-Δ10 nascent chain (NC) in cyan, YidC in red, and the DPPG/DPPC-based nanodisc in transparent orange. The reconstructed density was low-pass filtered at 7 Å.

(B) Molecular model of the RNC-bound YidC inserting the F_oc nascent chain (cyan) into the membrane. The individual helices of YidC are indicated in the top view (right). The positions of cross-linking residues within YidC (position 430) and F_oc (position 23) are shown in red.

(C) Conformational dynamics of YidC. The RNC-bound YidC (shown in colors) is overlaid on the reference crystal structure (PDB ID: 3WVF). The TM2, TM3, and EH1 helices undergo the largest shifts upon the ribosome binding and the nascent chain insertion. The cytoplasmic helical hairpin CH1-CH2 is suggested to shift laterally (black arrow) to open the central groove for the nascent chain insertion. See also Figures S3 and S4.

C-terminal tail of YidC that builds a primary contact with the ribosome (Kedrov et al., 2013; Seitl et al., 2014). Another contact site is resolved between ribosomal proteins L23/L29 and YidC TM4-TM5 positioned underneath, and the short loop that connects these two TMs has recently been shown to modulate ribosome binding (Geng et al., 2015). Additionally, we observe an extension at the ribosomal protein L24, which is large enough to fit up to three α-helical turns. Although no strong connection to the YidC core is resolved, the extension could be assigned to the part of the CH1-CH2 helical hairpin, the only cytoplasmic element missing in our model. In the idle state of YidC, the hairpin shields the central groove from the substrate access and would also sterically prevent the ribosome binding. When laterally shifted toward the L24 protein, the hairpin opens the path for the nascent chain, while not interfering with YidC:ribosome contact sites. The hairpin has previously been suggested to interact with the H59 RNA loop via residues Tyr-370 and Tyr-377 (Wickles et al., 2014). Though being lethal (Wickles et al., 2014), double mutation of these aromatic residues to alanines did not inhibit RNC F_oc binding (Figure S4E), thus questioning the role of the hairpin in ribosome binding.

Conformational Dynamics of YidC

The conformational difference of YidC between the idle and the ribosome-bound/inserting states observed here is mostly due to the tilting of TM2 and TM3 and the accompanying shift of the amphipathic helix EH1 toward the center of the membrane (Figures 5C and 6A). EH1 has been described as an essential part of YidC, as deletions in this region generated a lethal phenotype and inhibited YidC-mediated membrane insertion (Jiang et al., 2003; Kumazaki et al., 2014a). In agreement, we observed that removing a single helical turn (sequence LWFI) at the N-terminal end of EH1 had a strong suppressive effect on cell growth (Figure 6B), even though the ribosome binding in vitro was not affected. In the crystal structures of bacterial YidC, as well as that of a putative archaeal YidC homolog (Borowska et al., 2015), the EH1 helix appears at the membrane interface, with its N-terminal end slightly tilted toward the bilayer core. However, the YidC EH1 helix is largely hydrophobic and contains two solvent-oriented

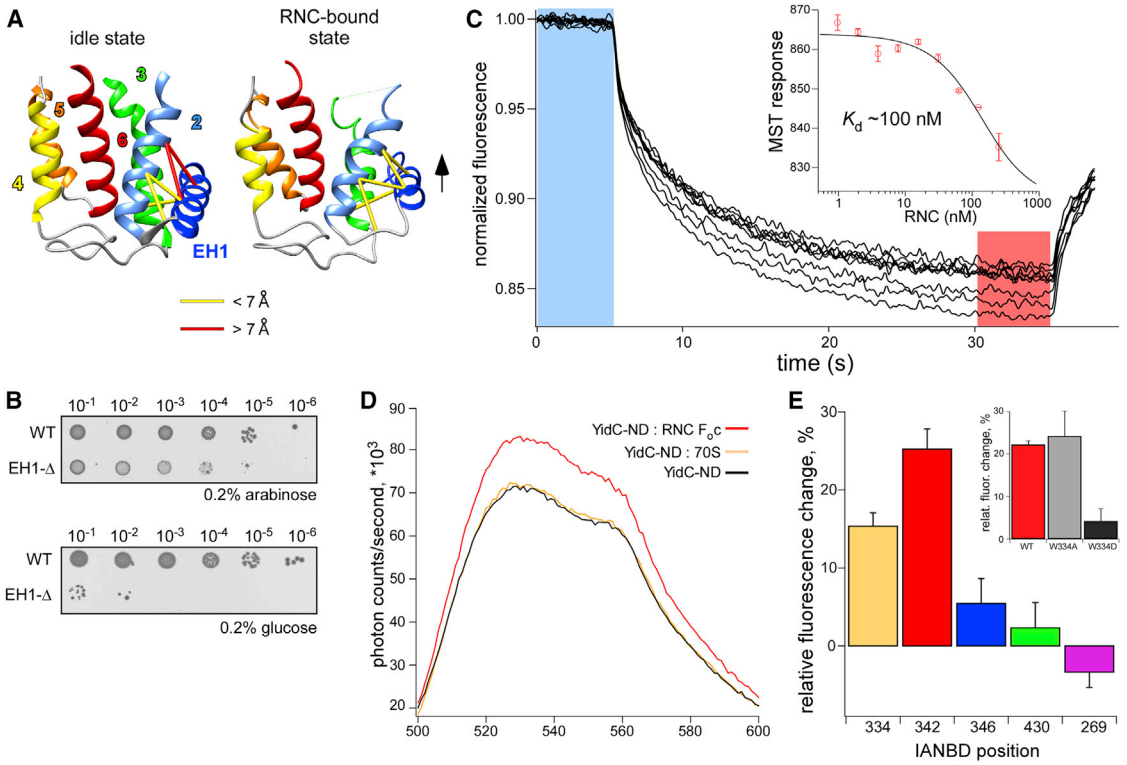

Figure 6. Structural Dynamics of YidC upon Membrane Protein Insertion

(A) The displacement of YidC amphipathic helix EH1 into the membrane upon RNC binding alters intramolecular distances between EH1 and TM2 helices (colored bars). A subset of evolutionary coupled residues in EH1 and TM2 achieve close contact in the RNC-bound conformation.

(B) Length of the EH1 helix is crucial for the cell viability. Deletion of four amino acids within the EH1 helix of YidC renders the protein non-functional and causes cell death.

(C) Microscale thermophoresis analysis of YidC$^{W334C, IANBD}$-ND interacting with RNC F_oc-Δ5. The raw traces (black) describe the efflux of YidC-ND from the high-temperature region, as the total fluorescence intensity decreases upon infrared (IR) illumination. The ratio of the fluorescence intensity after reaching the equilibrium in the temperature gradient (red) and prior IR illumination (blue) described the MST response of YidC-ND (inset) and was used for estimating the binding affinity.

(D) Emission spectra of EH1-conjugated IANBD upon YidC interactions with RNC F_oc-Δ5 or non-programmed ribosomes ("70S"). Adding RNCs resulted in the substantial increase of IANBD fluorescence, likely reflecting the dynamics of the EH1 helix.

(E) Relative changes in the fluorescence intensity of IANBD conjugated to different positions within YidC upon RNC F_oc-Δ5 binding, as measured at 540 nm (average fluorescence change + SD). Altering the hydrophobicity of the EH1 helix modulates its dynamics upon RNC binding (inset). An additional negative charge at position 334 strongly hinders the helix movement, as reflected by emission of IANBD fluorophore at position 342 measured at 540 nm. See also Figures S5 and S6.

lysines (Figure S5A), which when snorkeling (Strandberg and Killian, 2003), may allow the helix displacement toward the membrane core.

Statistical analysis on co-evolution of individual pairs of residues within a protein has recently provided a valuable tool to predict protein structure and dynamics, as a correlation between distant mutations often reflects residue contacts within the protein tertiary structure (de Juan et al., 2013; Ovchinnikov et al., 2014). Remarkably, several evolutionarily coupled residue pairs between EH1 and TM2; i.e., V351-I360, I347-I360, L343-I364, L344-S357, and I347-I364, are found among the highest scoring pairs within the protein (GREMLIN Server: http://www.openseq.org/ecoli.php?uni=P25714; Table S1), thus forming the most conserved region within the YidC structure and building a continuous coupling interface (Figures 6A and S5B), which is usually indicative of close physical proximity of domains. Notably, in the crystallized idle state of YidC, the distances between some of these paired residues are at the upper limit (7–8 Å for Cβ-Cβ atoms; Table S1). As co-evolutionary couplings have an intrinsic power to reflect both static and dynamic protein interactions (Sfriso et al., 2016), those contacts between EH1 and TM2 are potentially fulfilled in another conformation of the insertase. Indeed, in our cryo-EM model, they reside within an optimal range (below 7 Å; Figure 6A), suggesting that these paired residues approach each other in the RNC-bound form YidC.

To probe the potential dynamics of the EH1 helix and to test the structural model of ribosome-bound YidC, we introduced IANBD, an iodoacetamide derivate of the nitrobenzoxadiazole fluorophore, within EH1 (Figures S5D and S5E). As the fluorescence of IANBD increases in a hydrophobic environment, we reasoned that it could serve as a sensor for polarity of the EH1 moiety and report on the putative RNC-induced displacement

of the helix toward the lipid membrane core. Microscale thermophoresis (MST) (Seidel et al., 2013) analysis on IANBD-labeled YidC-ND showed pronounced changes in the MST response upon titrating RNC F_oc, but not non-translating 70S ribosomes, providing with dissociation constants in the range 50–100 nM (Figures 6C and S6). The environment-sensitive emission of IANBD was then measured for YidC in its free and RNC-bound states to probe the dynamics of the EH1 helix (Figures 6D and S5F). Only minor changes ranging from −5% to 5% were observed for IANBD at positions 269, 346, and 430, suggesting that the environment of these residues was barely affected upon RNC binding (Figure 6E). In contrast, a pronounced response was observed for IANBD at positions 334 and 342 of EH1, as the dye fluorescence increased 15 to 25% upon addition of RNCs, but not of empty 70S ribosomes (Figures 6D and 6E). Remarkably, the fluorescence change was sensitive to the net charge of EH1, as only minor increase in IANBD fluorescence was observed for the $YidC^{W334D}$ mutant upon RNC F_oc-Δ5 binding (Figure 6E, inset), while the RNC F_oc binding or cellular viability were not affected (Figures S5D and S5G). The net change-dependent increase in the fluorescence emission within EH1 suggested a transition of the helix toward the hydrophobic core of the membrane and thus experimentally supported the concept of the YidC conformational change as derived from the cryo-EM of the YidC:ribosome complex.

DISCUSSION

Molecular mechanisms of membrane protein biogenesis have been extensively studied over the last decade with a primary focus on functional dynamics of dedicated insertion machineries, the Sec translocon, and YidC-type insertases. Crystal structures of the YidC insertase in the membrane-mimetic environment (Kumazaki et al., 2014a, 2014b), together with a cryo-EM-based structure of YidC:ribosome complex in detergent (Wickles et al., 2014), revealed the molecular architecture of the insertase and have been used to suggest its functional mechanisms. Here, we employed YidC embedded within a lipid bilayer to explore the molecular determinants of the YidC:ribosome assembly and to reveal the structure of ribosome-bound YidC in the near physiological environment.

While incorporation of YidC into lipid bilayers stimulates interactions with translating ribosomes (Kedrov et al., 2013), we observed that YidC:ribosome binding depends only marginally on the particular lipid composition of tested model membranes. Thus, the recognition and initial assembly of the complex are likely determined by interacting surfaces of the ribosome, the nascent chain, and YidC, while the physical properties of the membrane environment fine-tune the interaction. However, our analysis on spontaneous and YidC-mediated insertion highlights the role of YidC in membranes rich of anionic lipids, thus pointing to the necessity of YidC-type insertases in bacterial and mitochondrial membranes, which contain large fractions of phosphatidylglycerol and cardiolipin lipids. Further, fluidity of the bilayer plays an important role in the downstream insertion and release of the nascent chain, as the cross-linking efficiency for YidC:nascent chain was substantially increased in gel phase membranes. Our analysis further shows that the YidC insertase is capable to recognize and insert relatively short hydrophobic domains of 15 amino acids emerging from a ribosome, but a specific investigation will be required to characterize the interplay between the nascent chain, YidC, and targeting factors, such as the signal recognition particle and its receptor (Facey et al., 2007; van Bloois et al., 2004).

Our cryo-EM structural analysis has provided a view on the architecture and dynamics of the YidC:RNC complex at near physiological conditions. The suggested structural model correlates with the previous study of the detergent-solubilized YidC:RNC complex (Wickles et al., 2014). In both environments, the C-terminal end of monomeric YidC interacts with the ribosomal RNA H59 and the short interhelical loop 4–5 of YidC builds a contact with L23/L29 ribosomal proteins. Also the position of the nascent chain egressing between YidC TM3 and TM5 is remarkably similar between two structures. However, the detergent-solubilized YidC core was described as a bundle of helices perpendicular to the membrane plane, while diverse tilts are observed in the membrane-based crystal structure and further tilting is described by our YidC-ND:RNC model. One explanation for the observed differences would be the low resolution of the previous cryo-EM study, which has been now improved by using a direct electron detector. Alternatively, different tilts of TM helices could be caused by the molecular environment, as the lateral forces built by lipidic cubic phases or the lipid bilayer within nanodiscs are very different from those in detergent micelles (Cross et al., 2013). Further, in our model, the essential CH1-CH2 hairpin of YidC is positioned in proximity to the ribosomal protein L24. The strong electron density earlier observed at the interface of detergent-solubilized YidC and ribosomal H59 and interpreted as the CH1-CH2 hairpin could be rather assigned to the 100 amino acid (aa) long and potentially structured C-terminal end of the YidC variant used in the previous study (Wickles et al., 2014).

The model of the YidC:ribosome complex suggests a large conformational change occurring in the membrane core of the insertase. While the C-terminal domain of YidC (TM4–TM6) resides normal to the membrane plane and determines ribosome binding, the N-terminal helices TM2 and TM3 tilt within the membrane plane by up to 20°. When compared to its idle state (Kumazaki et al., 2014b), the structure of the ribosome-bound YidC appears to be more open at the periplasmic side, so the polar N-terminal end of the nascent chain may be translocated somewhat orthogonally to the membrane plane, rather than via the "sliding" mechanism (Kumazaki et al., 2014a). The tilting of the TM2–TM3 pair is accompanied by relocating of the amphipathic EH1 helix into the hydrophobic membrane core. Though limited by the apparent flexibility and overall resolution ~10 Å, the structural model of the RNC-bound YidC is strongly supported by bioinformatics, and the biophysical analysis validated the proposed dynamic behavior of the YidC EH1 helix upon the nascent chain insertion. Interestingly, similar membrane relocating had been recently described for the amphipathic helix of the TatA subunit of the twin-arginine translocon, where the biophysical analysis in model membranes has been supported by an NMR-based structure (Chan et al., 2011; Rodriguez et al., 2013). Although EH1 of YidC has been suggested to reside at the membrane interface upon post-translational insertion (Imhof et al., 2011),

the dynamics of YidC upon ribosome binding and co-translational insertion observed here is clearly different.

For the observed dynamics of the essential YidC EH1 helix, we consider several hypotheses regarding its functional significance. The displacement of EH1 toward the membrane core is likely to cause further thinning of the lipid bilayer that could stimulate nascent chain insertion (Wickles et al., 2014). However, the close contacts of EH1 to the TM2/TM3 pair, together with the apparent length requirements of EH1, suggest that the helix may act as an intramolecular mechanical lever that coordinates a concerted movement resulting in tilting of TM3. This, in turn, may trigger release of the nascent chain from the polar core of YidC into the lipid environment due to a distortion of YidC's hydrophilic groove. In another scenario, binding of the ribosome and displacement of the helical hairpin CH1-CH2 may itself cause the conformational change within the insertase to allow the passage of the nascent chain into the lipid moiety. Here, it would be desirable to trap and visualize an insertion intermediate upon initial interaction with the hydrophilic core of YidC before partitioning into the lipid bilayer, so the dynamics of YidC over the whole functional cycle could be studied.

EXPERIMENTAL PROCEDURES

YidC Preparation

YidC overexpression plasmid pEM183 is based on pBAD-TOPO-TA (Thermo Fischer/Invitrogen) and encodes for full-length *E. coli* YidC in which the structurally disordered segment 206–215 (Oliver and Paetzel, 2008) has been replaced by eight histidine residues, resulting in an internal His_{10}-tag. Further point mutations and deletions within YidC were conducted via conventional molecular biology techniques, and resulting gene products were validated by sequencing (Eurofins Genomics). Recombinant YidC variants were expressed, purified, and optionally labeled following previously described protocols (Kedrov et al., 2013; Wickles et al., 2014) with minor modifications. *E. coli* ER2566 strain (New England Biolabs) was used for YidC overexpression upon induction with 0.2% arabinose at 37°C for 2 hr. Total membranes were isolated upon cell lysis and a sedimentation step. For YidC purification, the total membranes were solubilized in 1% Cymal 6, 300 mM NaCl, 200 μM TCEP, and 50 mM HEPES pH 7.2 and incubated with TALON beads (Clontech) at 4°C in presence 10 mM imidazole. Beads were washed with 40 mM imidazole to remove weakly and non-specifically bound proteins, and 300 mM imidazole was used to elute YidC. Optionally, prior to the elution step, single-cysteine variants of YidC were incubated with either 200 μM Alexa Fluor 488-C_5-maleimide or 400 μM NBD iodoacetamide (both Thermo Fischer/Molecular Probes) to achieve site-specific fluorescent labeling. All chemicals were purchased from Merck Millipore, Roth, or Sigma-Aldrich. Detergents were purchased from Affymetrix and Anatrace and solvent-solubilized lipids from Avanti Polar Lipids.

Nanodisc Preparation

MSP variants were expressed and purified as previously described (Kedrov et al., 2013; Ritchie et al., 2009). Prior to nanodisc assembly, lipids were destabilized with 0.5% Triton X-100, and DPPG/DPPC lipids were additionally incubated at 41°C. Nanodisc assembly was initiated by mixing YidC, MSP variants, and lipids at experimentally adjusted ratios, and detergents were removed by overnight incubation with Bio-Beads SM-2 sorbent (Bio-Rad). "Empty" and YidC-loaded nanodiscs were separated by size-exclusion chromatography on a Superdex 200 10/300 column (GE Life Sciences) in 150 mM KOAc, 5 mM $Mg(OAc)_2$, and 25 mM HEPES pH 7.2. For studying spontaneous insertion of F_oc into lipid-loaded nanodiscs, designed lipid mixtures were supplemented with 2% DOPE-Atto 488 fluorescent lipid derivative (ATTO-TEC GmbH). When necessary, nanodiscs were concentrated using Amicon Ultra Centrifugal Filters, MWCO 30 kDa (Merck Millipore).

A truncated variant of the major scaffold protein, MSP1D1-ΔH5, was designed according to a previous report (Hagn et al., 2013) by removing the region that encodes for the fifth helical domain (sequence PLRAELQEGARQKL HELQEKLS). Upon using the truncated MSP variant, the outer diameter of the nanodisc decreases by 13% from 9.7 nm to 8.4 nm, as previously determined in EM experiments (Hagn et al., 2013). Reduced dimensions of nanodiscs were validated in FCS measurements: The diffusion co-efficient of the truncated nanodisc increased by 12% from 49 ± 3 cm^2/s to 55 ± 4 cm^2/s (Figure S2), thus being inversely proportional to the diameter of the disc.

RNC Preparation

Translation-stalled RNCs were derived from the previously described construct F_oc-FL (Wickles et al., 2014), which nascent chain total length (including the C-terminal HA tag and the stalling TnaC sequence) closely matched the length of the fully synthesized F_oc protein (82 aa versus 79 aa, respectively). The F_oc fragment was further stepwise shortened from its C-terminal end resulting in nascent chains lacking 5 ("F_oc-Δ5", deleted sequence QPDLI), 10 ("F_oc-Δ10", EGAARQPDLI), and 20 ("F_oc-Δ20", GIGILGGKFLE GAARQPDLI) amino acids. RNCs were expressed and purified via metal-chelating chromatography using Ni^+-NTA beads (Clontech) as previously described (Bischoff et al., 2014b; Wickles et al., 2014). For better mimicking naturally occurring YidC substrates, 3C protease was used to remove N-terminal hexahistidine tags from the nascent chains after the affinity chromatography step, and 70S RNCs were subsequently isolated from 10%–40% linear sucrose gradients. At the final step RNCs were pelleted and resuspended in 150 mM KOAc, 5 mM Mg $(OAc)_2$, 0.03% DDM, and 25 mM HEPES pH 7.2 at concentration 3–5 μM and stored at −80°C.

Chemical Cross-Linking

Nanodisc-reconstituted YidC variants (approximately 1 μM) containing a single cysteine at position 430 in TM3 were incubated for 10 min at 30°C with 100 nM RNC F_oc containing a cysteine within the TM domain of the nascent chain. Fresh copper phenanthroline was added to concentration of 1 mM to induce cross-linking and the reaction was conducted for 20 min at 24°C. Optionally, formed disulphide bonds were reduced by adding 15 mM DTT and incubation at 30°C. For characterizing the cross-linking efficiency, reactions were loaded on non-reducing SDS-PAGE and the nascent chain in its free or cross-linked states was detected upon western blotting against the HA tag (Wickles et al., 2014).

Fluorescence Correlation Spectroscopy

FCS measurements were conducted using a home-built setup (Crevenna et al., 2013) as previously described (Geng et al., 2015), using fluorescent markers conjugated either to YidC or DOPE lipids. Each individual measurement was conducted for 100 s, so data from ~100,000 to ~300,000 diffusing molecules (average residence time ~300 μs) were accumulated to build an auto-correlation trace, and each measurement was repeated at least three times. Association of the YidC-ND (radius ~5 nm) with RNC F_oc (radius ~13 nm) slowed the translational diffusion of nanodiscs and prolonged their average residence time within the laser confocal volume of the FCS setup (Kedrov et al., 2013; Geng et al., 2015), so YidC-ND:ribosome interactions caused a shift of the auto-correlation curve along the time axis. Binding efficiencies were estimated from two-component fitting of auto-correlation traces, and diffusion coefficients/residence times of free nanodiscs and ribosomes were measured and used as parameters for fitting as previously described (Kedrov et al., 2013; Wu et al., 2012). For estimating the YidC:RNC affinity, RNCs were titrated within a specified range of concentrations, and for each RNC concentration the apparent residence time of YidC-ND was measured and normalized by the residence time of free YidC-ND. The measured dependence between normalized residence times and RNC concentrations was fitted with the single binding isotherm equation to estimate the dissociation constant.

Cryo-Electron Microscopy

For cryo-EM studies, 100 nM RNC F_oc-Δ10 were mixed with approximately 5-fold excess of pre-concentrated $YidC^{M430C}$-ND and 0.05% fluorinated octyl-maltoside (FOM) was added prior to loading the sample on the grid, as it has been described to stimulate uniform orientation of nanodiscs on the

carbon-coated grids (Efremov et al., 2015), while being non-disruptive for lipid bilayers (Popot, 2010). FCS measurements verified that FOM did not cause aggregation of lipid-based nanodiscs, and the YidC:ribosome complex was not affected. Samples were applied to carbon-coated holey grids according to standard methods (Wagenknecht et al., 1988). Direct electron detector Falcon II (FEI Company) was used for data acquisition with a final pixel size of 1.084 Å on the object scale. Micrographs were collected on FEI Titan Krios transmission electron microscope operating at 300 kV under low-dose conditions of 2.4 $e^-/Å^2$ per frame, nine frames in total. CTFFIND3 was used to determine defocus values and to estimate the resolution (Mindell and Grigorieff, 2003), while introducing a 5 Å resolution cutoff. Collected micrographs were further visually inspected to exclude aggregates or ice crystals. Single particles were picked from final 1,792 micrographs using the automated SIGNATURE software (Chen and Grigorieff, 2007) using ten representative projections of a 70S ribosome as references. Initial alignment of 3× binned data was performed using the SPIDER software package (Shaikh et al., 2008), providing an empty 70S ribosome as a reference, and resulted in a ribosome with strong densities for tRNA and a nanodisc. The alignment of the data set was further refined and non-ribosomal particles were removed upon SPIDER-based sorting, resulting in a data set of 144,976 ribosomal particles. These particles were extracted with Relion software (Scheres, 2012) and further processed using the FREALIGN v9.11 software (Grigorieff, 2007). All sorting steps were carried out on 3× binned data. Initial sorting into five classes allowed us to discard both 50S subunits and ribosomes bound to additional factors. Further sorting using a 3D mask covering the 50S subunit and the disc allowed us to discard ribosomes with weak densities for the nanodisc and ribosomes with a strong orientation bias. The alignment of the remaining 42,658 RNC:nanodisc particles was refined using unbinned data, reaching the final resolution $FSC_{0.143}$ = 3.8 Å for the large ribosomal subunit and 4.5 Å for the complex with YidC-ND, as measured by the Relion software. The map used for YidC structure refinements was B-factor sharpened using bfactor.exe of the FREALIGN distribution and filtered to 7 Å.

Helical densities corresponding to TM helices of YidC and the inserted nascent chain were separated from the unstructured and fuzzy density of the surrounding lipids of the nanodisc. The YidC crystal structure of *E. coli* was fitted into strong densities in proximity to the ribosomal tunnel. The C-terminal part of YidC (TM4–TM6) was placed as a rigid body into helical densities that extend from the membrane to form contacts with the ribosomal protein L23/L29 and the RNA loop H59. The initial fit was further improved by adjusting positions of N-terminal helices EH1, TM2, and TM3 individually: TM2 and TM3 were tilted within the membrane plane and an additional vertical shift was introduced for the amphipathic helix EH1. In comparison to the functional core of the protein, the extramembrane part of YidC was poorly resolved, in agreement with higher B-factor values observed in crystallographic studies (Kumazaki et al., 2014b) and earlier cryo-EM analysis conducted in the detergent environment (Seitl et al., 2014; Wickles et al., 2014). High flexibility of the periplasmic P1 domain that connects TM1 to the conserved core might contribute to the diffuse and unresolved density for both entities. The N-terminal transmembrane fragment of F_oc (residues LYMAAAVMMGLAAIGAAIGIG; PDB ID: 1C99; Rastogi and Girvin, 1999) was fitted to the additional rod-like density at the YidC:lipid interface. YidC model was further refined using Phenix software (Adams et al., 2010). To test the validity of the built model, FSC between the experimental volume and the map of the model created with pdb2mrc command in EMAN2 (Tang et al., 2007) was calculated using Relion.

IANBD Fluorescence and Analysis

IANBD, whose structure closely mimics the tryptophan side chain, was introduced at non-conserved positions of Trp-334, Lys-342, or Trp-346 within the EH1 helix (Figure S5). Alternatively, IANBD was conjugated either at the membrane-embedded position 430 or the solvent-exposed position 269 within the P1 domain. IANBD-labeled YidC variants were reconstituted into lipid-based nanodiscs containing 35 mol % DPPG and 65 mol % DPPC and the fluorophore emission spectra were recorded using FluoroMax-2 spectrophotometer (HORIBA Jobin Yvon) at 22°C. The excitation wavelength was set to 470 nm and the emission spectra were recorded between 500 and 600 nm. $YidC^{IANBD}$-ND was diluted to ~30 nM and mixed with either RNC F_oc-Δ5, non-translating 70S ribosomes, or the corresponding volume of ribosome-free buffer. Background ribosome-related scattering was accounted for by recording the spectra in absence of YidC-ND and subtracting that from the IANBD spectra. The change in IANBD fluorescence caused by interactions with ribosomes was derived by calculating a difference between the spectra in presence and absence of ribosomes and the values at 540 nm were used to calculate the relative change.

Microscale Thermophoresis

MST measurements on $YidC^{IANBD}$-ND:RNC F_oc-Δ5 were conducted following the conventional experimental scheme. Briefly, series of RNC titration from 500 nM to 2 nM were prepared and mixed with equal volumes of $YidC^{IANBD}$-ND, so the final concentration of YidC was approximately 30 nM. After 5 min incubation at 24°C, samples were loaded in "Premium" coated capillaries (NanoTemper Technologies) and subjected to the MST analysis. Stability of YidC-ND was evaluated by performing capillary scanning before and after the measurements. Stability of RNCs was evaluated in independent measurements using Alexa Fluor 488-labeled ribosomes (Beckert et al., 2015). Experiments were conducted using a Monolith NT.115 instrument (NanoTemper Technologies) at 24°C and employing the blue LED illumination. Infrared laser power was set to 20%, 40%, or 60% and data recorded at 40% was used for further analysis.

ACCESSION NUMBERS

The accession numbers for the cryo-EM map of the RNC:YidC-ND complex and the molecular model of YidC reported in this paper are Electron Microscopy Data Bank: EMDB-4155 and PDB: 5M5H.

SUPPLEMENTAL INFORMATION

Supplemental Information includes Supplemental Experimental Procedures, six figures, and one table and can be found with this article online at http://dx.doi.org/10.1016/j.celrep.2016.11.059.

AUTHOR CONTRIBUTIONS

Research Design: A.K., S.W., and R.Beckmann. Molecular Biology and Biochemistry: A.K., E.O.v.d.S., and R.Buschauer. Biophysical Experiments and Analysis: A.K., A.H.C., R.Buschauer, and D.C.L. Cryo-EM Experiments: O.B. Cryo-EM Analysis: A.K., S.W., and R.Beckmann. Manuscript Preparation: A.K. with contribution of all co-authors.

ACKNOWLEDGMENTS

We thank Joanna Musial for the technical assistance with protein biochemistry; Susanne Rieder and Charlotte Ungewickell for preparing samples for cryo-EM; André Heuer, Christian Schmidt, Bertrand Beckert, and Jingdong Cheng for assistance in cryo-EM analysis; Lukas Bischoff for valuable discussions on the project; and Daniel N. Wilson for the careful reading and commenting on the manuscript. The project was supported by the ERC Advanced Investigator grant "Cryotranslation" to R.Beckmann and Deutsche Forschungsgemeinschaft (DFG) Research grant (KE 1879/3-1) to A.K. D.C.L. gratefully acknowledges the financial support of DFG through the SFB 646, the Clusters of Excellence Nanosystems Initative Munich and Center for Integrated Protein Science Munich, and the Ludwig-Maximilians-University Munich via the LMUInnovativ BioImaging Network and the Center for NanoScience.

Received: June 3, 2016
Revised: October 26, 2016
Accepted: November 20, 2016
Published: December 13, 2016

REFERENCES

Adams, P.D., Afonine, P.V., Bunkóczi, G., Chen, V.B., Davis, I.W., Echols, N., Headd, J.J., Hung, L.W., Kapral, G.J., Grosse-Kunstleve, R.W., et al. (2010).

PHENIX: A comprehensive Python-based system for macromolecular structure solution. Acta Crystallogr. Sect. D Biol. Crystallogr. *66*, 213–221.

Beckert, B., Kedrov, A., Sohmen, D., Kempf, G., Wild, K., Sinning, I., Stahlberg, H., Wilson, D.N., and Beckmann, R. (2015). Translational arrest by a prokaryotic signal recognition particle is mediated by RNA interactions. Nat. Struct. Mol. Biol. *22*, 767–773.

Bischoff, L., Berninghausen, O., and Beckmann, R. (2014a). Molecular basis for the ribosome functioning as an L-tryptophan sensor. Cell Rep. *9*, 469–475.

Bischoff, L., Wickles, S., Berninghausen, O., van der Sluis, E.O., and Beckmann, R. (2014b). Visualization of a polytopic membrane protein during SecY-mediated membrane insertion. Nat. Commun. *5*, 4103.

Borowska, M.T., Dominik, P.K., Anghel, S.A., Kossiakoff, A.A., and Keenan, R.J. (2015). A YidC-like protein in the archaeal plasma membrane. Structure *23*, 1715–1724.

Chan, C.S., Haney, E.F., Vogel, H.J., and Turner, R.J. (2011). Towards understanding the Tat translocation mechanism through structural and biophysical studies of the amphipathic region of TatA from Escherichia coli. Biochim. Biophys. Acta *1808*, 2289–2296.

Chen, J.Z., and Grigorieff, N. (2007). SIGNATURE: a single-particle selection system for molecular electron microscopy. J. Struct. Biol. *157*, 168–173.

Chen, Y., Soman, R., Shanmugam, S.K., Kuhn, A., and Dalbey, R.E. (2014). The role of the strictly conserved positively charged residue differs among the Gram-positive, Gram-negative, and chloroplast YidC homologs. J. Biol. Chem. *289*, 35656–35667.

Crevenna, A.H., Naredi-Rainer, N., Schönichen, A., Dzubiella, J., Barber, D.L., Lamb, D.C., and Wedlich-Söldner, R. (2013). Electrostatics control actin filament nucleation and elongation kinetics. J. Biol. Chem. *288*, 12102–12113.

Cronan, J.E. (2003). Bacterial membrane lipids: where do we stand? Annu. Rev. Microbiol. *57*, 203–224.

Cross, T.A., Murray, D.T., and Watts, A. (2013). Helical membrane protein conformations and their environment. Eur. Biophys. J. *42*, 731–755.

de Juan, D., Pazos, F., and Valencia, A. (2013). Emerging methods in protein co-evolution. Nat. Rev. Genet. *14*, 249–261.

Denisov, I.G., Grinkova, Y.V., Lazarides, A.A., and Sligar, S.G. (2004). Directed self-assembly of monodisperse phospholipid bilayer Nanodiscs with controlled size. J. Am. Chem. Soc. *126*, 3477–3487.

du Plessis, D.J., Nouwen, N., and Driessen, A.J.M. (2011). The Sec translocase. Biochim. Biophys. Acta *1808*, 851–865.

Efremov, R.G., Leitner, A., Aebersold, R., and Raunser, S. (2015). Architecture and conformational switch mechanism of the ryanodine receptor. Nature *517*, 39–43.

Facey, S.J., Neugebauer, S.A., Krauss, S., and Kuhn, A. (2007). The mechanosensitive channel protein MscL is targeted by the SRP to the novel YidC membrane insertion pathway of Escherichia coli. J. Mol. Biol. *365*, 995–1004.

Frauenfeld, J., Gumbart, J., Sluis, E.O., Funes, S., Gartmann, M., Beatrix, B., Mielke, T., Berninghausen, O., Becker, T., Schulten, K., and Beckmann, R. (2011). Cryo-EM structure of the ribosome-SecYE complex in the membrane environment. Nat. Struct. Mol. Biol. *18*, 614–621.

Gao, Y., Cao, E., Julius, D., and Cheng, Y. (2016). TRPV1 structures in nanodiscs reveal mechanisms of ligand and lipid action. Nature *534*, 347–351.

Geng, Y., Kedrov, A., Caumanns, J.J., Crevenna, A.H., Lamb, D.C., Beckmann, R., and Driessen, A.J.M. (2015). Role of the cytosolic loop C2 and the C terminus of YidC in ribosome binding and insertion activity. J. Biol. Chem. *290*, 17250–17261.

Grigorieff, N. (2007). FREALIGN: high-resolution refinement of single particle structures. J. Struct. Biol. *157*, 117–125.

Hagn, F., Etzkorn, M., Raschle, T., and Wagner, G. (2013). Optimized phospholipid bilayer nanodiscs facilitate high-resolution structure determination of membrane proteins. J. Am. Chem. Soc. *135*, 1919–1925.

Imhof, N., Kuhn, A., and Gerken, U. (2011). Substrate-dependent conformational dynamics of the Escherichia coli membrane insertase YidC. Biochemistry *50*, 3229–3239.

Jiang, F., Chen, M., Yi, L., de Gier, J.W., Kuhn, A., and Dalbey, R.E. (2003). Defining the regions of Escherichia coli YidC that contribute to activity. J. Biol. Chem. *278*, 48965–48972.

Kedrov, A., Sustarsic, M., de Keyzer, J., Caumanns, J.J., Wu, Z.C., and Driessen, A.J.M. (2013). Elucidating the native architecture of the YidC: ribosome complex. J. Mol. Biol. *425*, 4112–4124.

Krichevsky, O., and Bonnet, G. (2002). Fluorescence correlation spectroscopy: the technique and its applications. Rep. Prog. Phys. *65*, 251–297.

Kucharska, I., Edrington, T.C., Liang, B., and Tamm, L.K. (2015). Optimizing nanodiscs and bicelles for solution NMR studies of two β-barrel membrane proteins. J. Biomol. NMR *61*, 261–274.

Kumazaki, K., Chiba, S., Takemoto, M., Furukawa, A., Nishiyama, K., Sugano, Y., Mori, T., Dohmae, N., Hirata, K., Nakada-Nakura, Y., et al. (2014a). Structural basis of Sec-independent membrane protein insertion by YidC. Nature *509*, 516–520.

Kumazaki, K., Kishimoto, T., Furukawa, A., Mori, H., Tanaka, Y., Dohmae, N., Ishitani, R., Tsukazaki, T., and Nureki, O. (2014b). Crystal structure of Escherichia coli YidC, a membrane protein chaperone and insertase. Sci. Rep. *4*, 7299.

Mindell, J.A., and Grigorieff, N. (2003). Accurate determination of local defocus and specimen tilt in electron microscopy. J. Struct. Biol. *142*, 334–347.

Oliver, D.C., and Paetzel, M. (2008). Crystal structure of the major periplasmic domain of the bacterial membrane protein assembly facilitator YidC. J. Biol. Chem. *283*, 5208–5216.

Ovchinnikov, S., Kamisetty, H., and Baker, D. (2014). Robust and accurate prediction of residue-residue interactions across protein interfaces using evolutionary information. eLife *3*, e02030.

Park, E., and Rapoport, T.A. (2012). Mechanisms of Sec61/SecY-mediated protein translocation across membranes. Annu. Rev. Biophys. *41*, 21–40.

Popot, J.-L. (2010). Amphipols, nanodiscs, and fluorinated surfactants: three nonconventional approaches to studying membrane proteins in aqueous solutions. Annu. Rev. Biochem. *79*, 737–775.

Rastogi, V.K., and Girvin, M.E. (1999). Structural changes linked to proton translocation by subunit c of the ATP synthase. Nature *402*, 263–268.

Ritchie, T.K., Grinkova, Y.V., Bayburt, T.H., Denisov, I.G., Zolnerciks, J.K., Atkins, W.M., and Sligar, S.G. (2009). Chapter 11 - Reconstitution of membrane proteins in phospholipid bilayer nanodiscs. Methods Enzymol. *464*, 211–231.

Rodriguez, F., Rouse, S.L., Tait, C.E., Harmer, J., De Riso, A., Timmel, C.R., Sansom, M.S.P., Berks, B.C., and Schnell, J.R. (2013). Structural model for the protein-translocating element of the twin-arginine transport system. Proc. Natl. Acad. Sci. USA *110*, E1092–E1101.

Saller, M.J., Wu, Z.C., de Keyzer, J., and Driessen, A.J.M. (2012). The YidC/Oxa1/Alb3 protein family: common principles and distinct features. Biol. Chem. *393*, 1279–1290.

Samuelson, J.C., Chen, M., Jiang, F., Möller, I., Wiedmann, M., Kuhn, A., Phillips, G.J., and Dalbey, R.E. (2000). YidC mediates membrane protein insertion in bacteria. Nature *406*, 637–641.

Scheres, S.H.W. (2012). RELION: implementation of a Bayesian approach to cryo-EM structure determination. J. Struct. Biol. *180*, 519–530.

Scotti, P.A., Urbanus, M.L., Brunner, J., de Gier, J.W., von Heijne, G., van der Does, C., Driessen, A.J.M., Oudega, B., and Luirink, J. (2000). YidC, the Escherichia coli homologue of mitochondrial Oxa1p, is a component of the Sec translocase. EMBO J. *19*, 542–549.

Seidel, S.A.I., Dijkman, P.M., Lea, W.A., van den Bogaart, G., Jerabek-Willemsen, M., Lazic, A., Joseph, J.S., Srinivasan, P., Baaske, P., Simeonov, A., et al. (2013). Microscale thermophoresis quantifies biomolecular interactions under previously challenging conditions. Methods *59*, 301–315.

Seitl, I., Wickles, S., Beckmann, R., Kuhn, A., and Kiefer, D. (2014). The C-terminal regions of YidC from Rhodopirellula baltica and Oceanicaulis alexandrii bind to ribosomes and partially substitute for SRP receptor function in Escherichia coli. Mol. Microbiol. *91*, 408–421.

Sfriso, P., Duran-Frigola, M., Mosca, R., Emperador, A., Aloy, P., and Orozco, M. (2016). Residues coevolution guides the systematic identification of alternative functional conformations in proteins. Structure *24*, 116–126.

Shaikh, T.R., Gao, H., Baxter, W.T., Asturias, F.J., Boisset, N., Leith, A., and Frank, J. (2008). SPIDER image processing for single-particle reconstruction of biological macromolecules from electron micrographs. Nat. Protoc. *3*, 1941–1974.

Strandberg, E., and Killian, J.A. (2003). Snorkeling of lysine side chains in transmembrane helices: how easy can it get? FEBS Lett. *544*, 69–73.

Tang, G., Peng, L., Baldwin, P.R., Mann, D.S., Jiang, W., Rees, I., and Ludtke, S.J. (2007). EMAN2: an extensible image processing suite for electron microscopy. J. Struct. Biol. *157*, 38–46.

van Bloois, E., Jan Haan, G., de Gier, J.W., Oudega, B., and Luirink, J. (2004). F(1)F(0) ATP synthase subunit c is targeted by the SRP to YidC in the E. coli inner membrane. FEBS Lett. *576*, 97–100.

van der Laan, M., Bechtluft, P., Kol, S., Nouwen, N., and Driessen, A.J.M. (2004). F1F0 ATP synthase subunit c is a substrate of the novel YidC pathway for membrane protein biogenesis. J. Cell Biol. *165*, 213–222.

Wagenknecht, T., Grassucci, R., and Frank, J. (1988). Electron microscopy and computer image averaging of ice-embedded large ribosomal subunits from Escherichia coli. J. Mol. Biol. *199*, 137–147.

Wickles, S., Singharoy, A., Andreani, J., Seemayer, S., Bischoff, L., Berninghausen, O., Soeding, J., Schulten, K., van der Sluis, E.O., and Beckmann, R. (2014). A structural model of the active ribosome-bound membrane protein insertase YidC. eLife *3*, e03035.

Wu, Z.C., de Keyzer, J., Kedrov, A., and Driessen, A.J.M. (2012). Competitive binding of the SecA ATPase and ribosomes to the SecYEG translocon. J. Biol. Chem. *287*, 7885–7895.

Wu, Z.C., de Keyzer, J., Berrelkamp-Lahpor, G.A., and Driessen, A.J.M. (2013). Interaction of Streptococcus mutans YidC1 and YidC2 with translating and nontranslating ribosomes. J. Bacteriol. *195*, 4545–4551.

Yu, Z., Koningstein, G., Pop, A., and Luirink, J. (2008). The conserved third transmembrane segment of YidC contacts nascent Escherichia coli inner membrane proteins. J. Biol. Chem. *283*, 34635–34642.

Cell Reports, Volume *17*

Supplemental Information

Structural Dynamics of the YidC:Ribosome Complex during Membrane Protein Biogenesis

Alexej Kedrov, Stephan Wickles, Alvaro H. Crevenna, Eli O. van der Sluis, Robert Buschauer, Otto Berninghausen, Don C. Lamb, and Roland Beckmann

Supplemental Figures

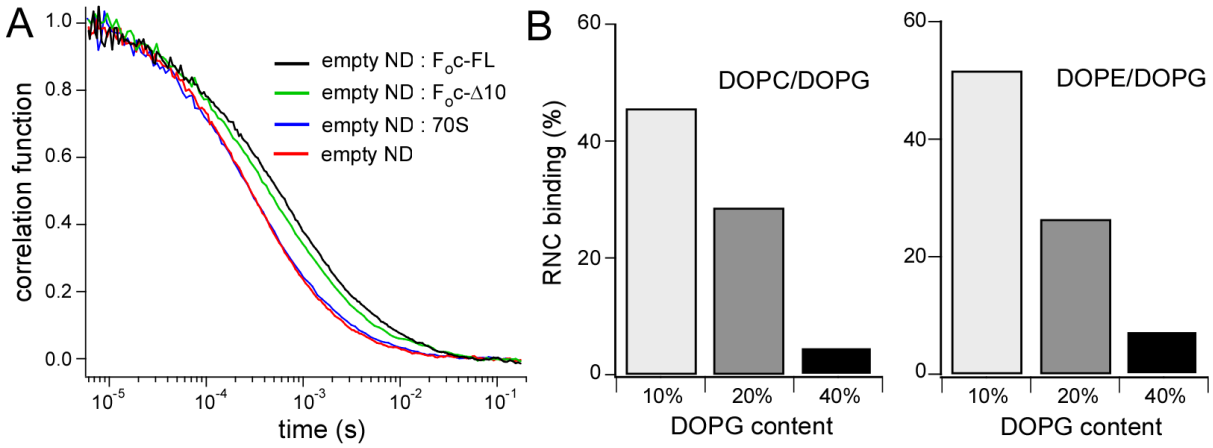

Figure S1. Related to the Figure 2. Spontaneous membrane insertion of F_oc depends on the lipid composition. Spontaneous insertion of hydrophobic nascent chains in the lipid bilayer is a potential pathway occurring in parallel to YidC-mediated insertion. (A) Auto-correlation curves of empty, YidC-free, nanodiscs (98% DOPC, 2% DOPE-Atto 488) diffusing in absence and presence of 200 nM RNC F_oc. The slower diffusion of nanodiscs reflects spontaneous binding of RNCs in absence of anionic lipids, such as DOPG. No interaction can be detected between nanodiscs and non-translating 70S ribosomes. Thus, the RNC binding is mainly mediated by the F_oc nascent chain, the hydrophobic domain of which likely partitioned spontaneously into the membrane. (B) The efficiency of the spontaneous YidC-independent insertion of F_oc into the membrane depends on the content of anionic lipids DOPG. Incorporation of YidC into nanodiscs will likely reduce the spontaneous insertion due to steric constraints at the membrane interface and the excluded volume within the lipid bilayer. FCS recordings were conducted in presence of 50 nM RNC F_oc-FL and the binding efficiency was calculated from the two-component model fitting.

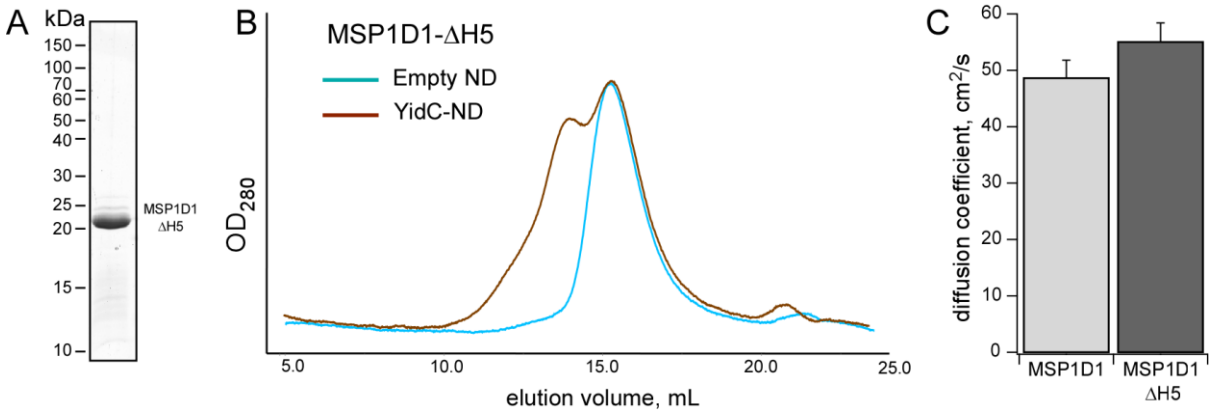

Figure S2. Related to the main text and Figure 4. Characterization of MSP1D1-ΔH5 nanodiscs. (A) SDS-PAGE of over-expressed and purified MSP1D1-ΔH5 variant. (B) Size-exclusion chromatography profile of empty and YidC-loaded nanodiscs formed by the MSP1D1-ΔH5 variant. (C) Lipid-loaded nanodiscs formed by the truncated MSP variant demonstrated higher diffusion coefficient than the original MSP1D1-based nanodiscs in agreement with the reduction in size (average diff. coef. + s.d.).

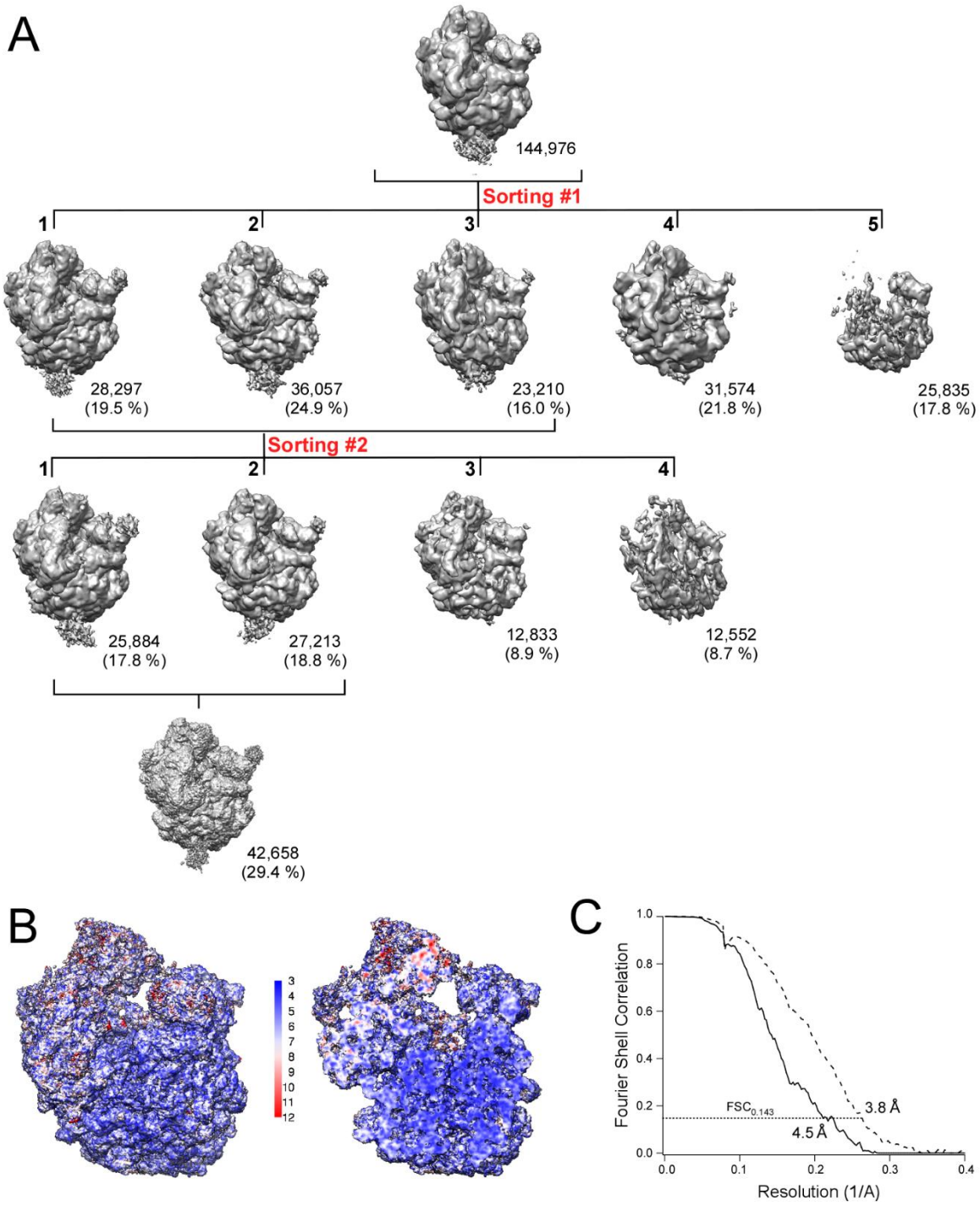

Figure S3. Related to Figure 5. Cryo-EM of the YidC-ND:RNC complex. (A) Sorting scheme of the cryo-EM data. The initial dataset of ribosomal particles displayed a strong density at the tunnel exit. FREALIGN-based sorting into 5 classes ("Sorting #1") allowed to separate partially dissociated ribosome (class 5) and ribosomes bound to other factors or occasional non-ribosomal particles (class 4). Classes 1 and 2 represented slightly different conformations of the ribosome, and class 3 demonstrated certain bias in orientation of particles. Classes 1-3 were merged and further sorted using a mask built of the large ribosomal subunit (50S) and a cylindrical density at the tunnel exit ("Sorting #2"). Dimensions of the masking cylinder exceeded the nanodisc approx. 2.5 fold. The sorting allowed

excluding particles with a strong orientation bias (class 4) and with a weak density for YidC-ND (class 3). Remaining classes 1 and 2 differed by an extension of YidC-ND, probably reflecting orientations of non-essential periplasmic P1 domain. These classes were merged and used for further refinement and modelling. The number of particles and its fraction in the initial data set (%) is indicated for each class. (B) Local resolution of the cryo-EM ribosome structure. Local resolution map of the surface (left) and interior (right) of the RNC F_oc-Δ10. The large ribosomal subunit (50S) was used for alignment of the dataset, resulting in a higher local resolution for the subunit. (C) FSC curves for 50S ribosomal subunit used for alignment (dashed line) and for the complex with YidC-ND (solid line). Corresponding average resolution values at $FSC_{0.143}$ are indicated.

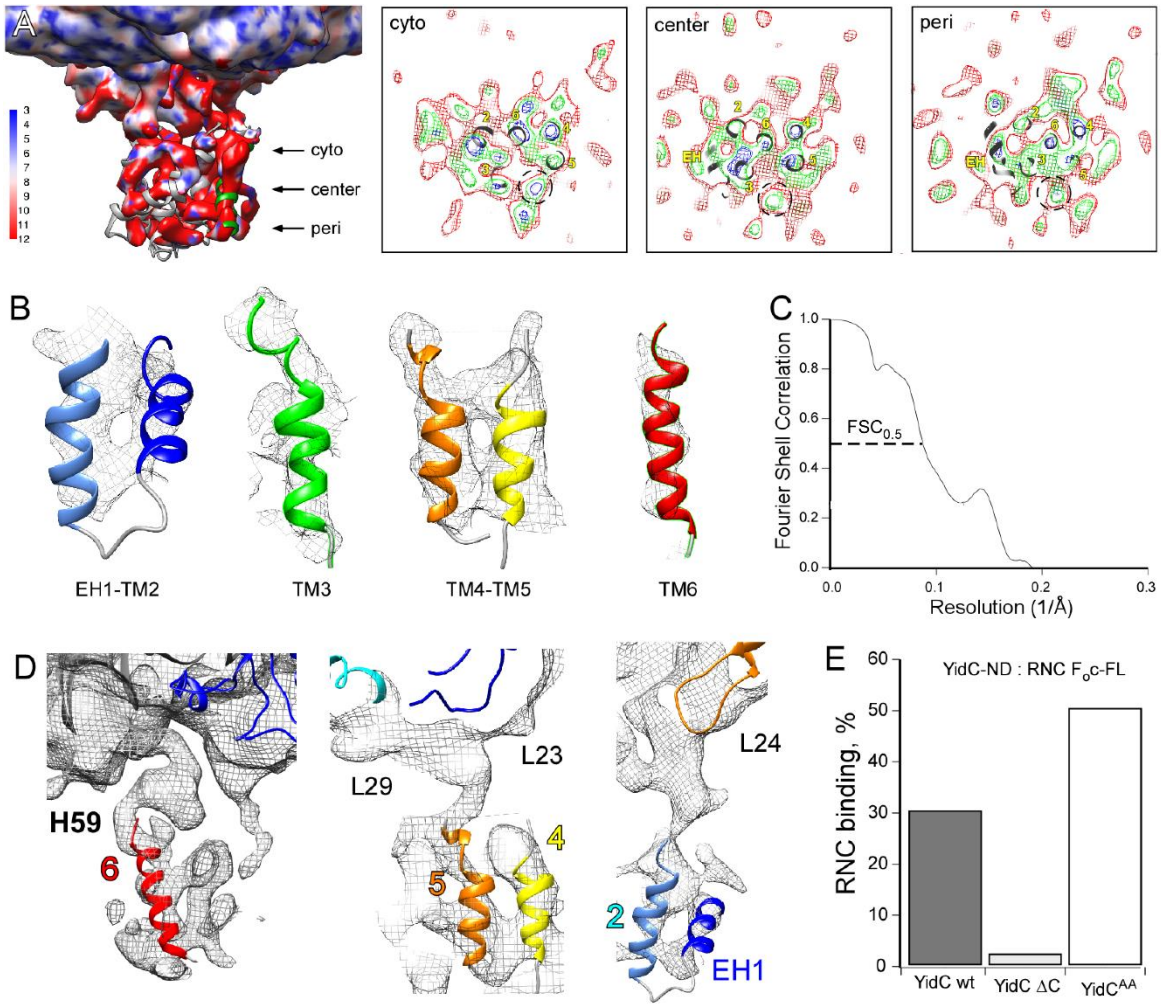

Figure S4. Related to Figure 5. Modelling the structure of YidC. (A) The local resolution map of YidC-ND reflects its higher flexibility compared to the ribosomal proteins. For modeling the YidC conformation its transmembrane helices were fitted in most prominent densities at the center of the nanodisc. Positioning of the helices within densities through the membrane plane at different levels (shown in blue/green/red) is shown on panels (right). (B) Fitting of YidC helices into cryo-EM densities. (C) FSC curve of model vs. map of nanodisc-embedded YidC. $FSC_{0.5}$ value of ~10 Å agrees with the limited local resolution of YidC-ND. (D) Primary contacts of YidC with the ribosome. The major contact site is built by C-terminal end of TM6 and the ribosomal RNA loop H59. Large density at the end of YidC TM6 may reflect the partially folded C-terminus. Short loop between YidC TM4 and TM5 approaches ribosomal protein L29 and L23. The pronounced extension near the ribosomal protein L24 likely reflects the position of YidC CH1-CH2 helical hairpin. (E) Mutations in the CH1-CH2 hairpin of YidC do not inhibit RNC binding. Nanodisc-reconstituted $YidC^{Y370A, Y377A}$ ($YidC^{AA}$) efficiently binds RNC F_oc-FL (50 nM) as tested by means of FCS.

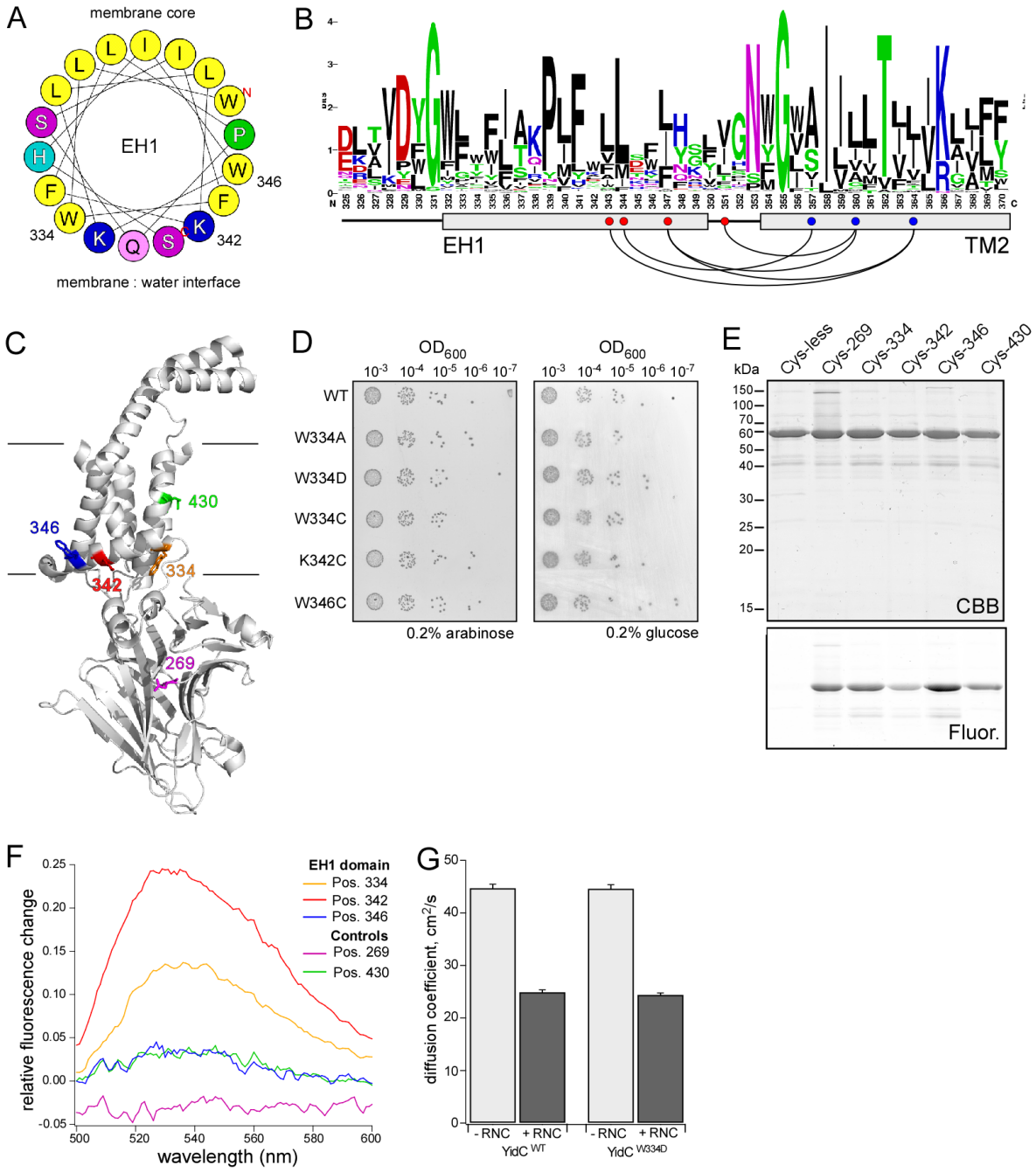

Figure S5. Related to Figure 6. Structural dynamics of the EH1 helix. (A) The wheel plot illustrates the amphipathic structure of the YidC EH1 helix, with a broad hydrophobic lipid-exposed interface (top), and a few polar/charged residues oriented towards the aqueous solvent (bottom). Positions of the IANBD fluorophore conjugated within EH1 are indicated. The wheel plot was generated using the HeliQuest server: http://heliquest.ipmc.cnrs.fr. (B) The sequence logo of the YidC EH1-TM2 region and evolutionarily coupled residues within. The sequence logo was generated using the WebLogo server: http://weblogo.berkeley.edu (C) Positions of the IANBD fluorophore conjugated to YidC are shown on the crystal structure of YidC in its idle state. (D) Point mutations within the EH1 helix do not affect the *in vivo* functionality of YidC. (E) Specificity of IANBD conjugation via the thioether bond was confirmed using a cysteine-less YidC variant as a negative control in the

labeling reaction. Occasional low-MW bands seen in SDS-PAGE likely originate from limited YidC degradation, as using cysteine-less YidC also prevented their labeling with IANBD. (F) Relative changes in IANBD fluorescence upon RNC F_oc-Δ5 binding depend on the fluorophore position. Variations in IANBD fluorescence levels between different positions within EH1 can be explained based on the structure of YidC: The transfer from the lipid head-group region to the acyl chains moiety upon ribosome binding should cause large changes in the polarity for the membrane interface-oriented residues 334 and 342. In contrast, the residue 346 is initially oriented towards the hydrophobic membrane core (A), and hence changes in the polarity and the associated IANBD fluorescence upon the EH1 displacement are substantially lower for this position. (G) An additional negative charge introduced into EH1 by mutation W334D does not affect RNC binding (diff. coef. + s.d.). The binding assay was performed by means of FCS using AlexaFluor 488-labeled $YidC^{D269C}$ variants in DPPG/DPPC-based nanodiscs and 150 nM RNC F_oc-FL.

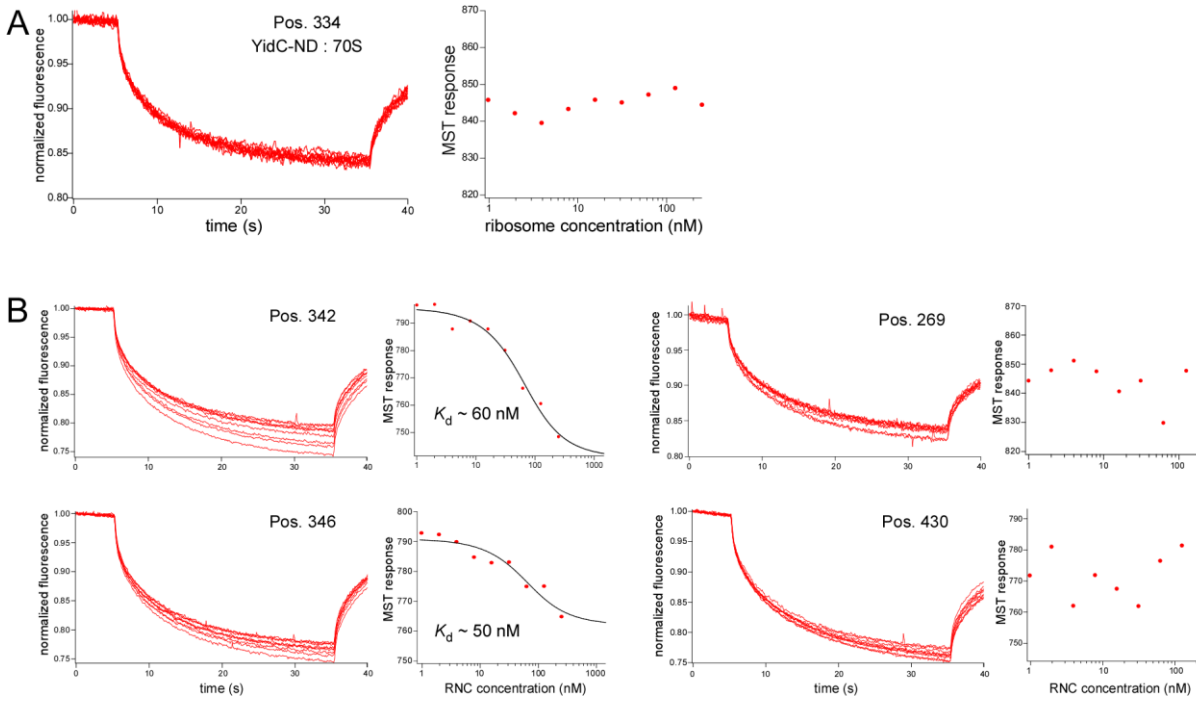

Figure S6. Related to Figure 6. Microscale thermophoresis on YidC^{IANBD}-ND: ribosome interactions. (A) The MST response of nanodisc-reconstituted YidC^{IANBD} is not affected by non-translating 70S ribosomes in agreement with the extremely low affinity. Left: normalized time-lapse fluorescence recordings; right: calculated fluorescence change, i.e. MST response upon local heating and thermal diffusion of fluorescently labeled YidC. (B) IANBD, an environment-sensitive dye conjugated within the EH1 helix (positions 342 and 346) allows resolving assembly of the YidC-ND:RNC complex, as the MST response is dependent on the RNC F_oc-Δ5 concentration. Notably, the MST response depended on the IANBD conjugation site within EH1, being the strongest for the position 342 and the weakest for 346 that correlates with IANBD fluorescence increase (Fig. 6). No interaction could be resolved when the dye is conjugated either at a solvent-exposed (position 269), or a statically buried within the membrane sites (position 430), that is likely due to a mutual compensation of several MST determinants, such as size and charge distribution.

Table S1. Related to Figure 6. Co-evolution of EH1-TM2 helices. A set of distanced residues in EH1 and TM2 form evolutionary conserved pairs within the YidC structure (highlighted in orange) and presumably build the interaction interface. Distances between Cβ atoms of those have been measured using the crystal structure of *E.coli* YidC (Kumazaki et al., 2014b). The co-evolution analysis data was adopted from David Baker's lab (http://gremlin.bakerlab.org/ecoli.php?uni=P25714), and residues separated by less than 6 positions in the primary sequence have been omitted from the table.

Res1	Res2	probability	distance, Å	new dist., Å	distance, aa
64	85	1			21
351	360	1	6.7	6.1	9
386	417	1			31
356	451	1			95
393	404	0.999			11
369	432	0.998			63
472	503	0.998			31
347	360	0.997	5.1	5.4	13
343	364	0.995	7.4	6.4	21
82	309	0.993			227
72	151	0.991			79
162	179	0.989			17
65	167	0.988			102
356	452	0.978			96
63	167	0.974			104
467	515	0.974			48
70	82	0.972			12
470	518	0.966			48
77	151	0.96			74
344	357	0.951	5.3	6.7	13
261	327	0.945			66
471	503	0.945			32
394	404	0.942			10
69	83	0.931			14
70	167	0.924			97
369	428	0.921			59
179	302	0.919			123
66	170	0.911			104
455	467	0.902			12
347	364	0.896	8.1	5.9	17
173	320	0.881			147
365	428	0.879			63
469	500	0.876			31